Influence of start-up phase of an incinerator on inorganic composition and lead isotope ratios of the atmospheric PM10

Published version:

DOI:10.1016/j.chemosphere.2020.129091

Influence of start-up phase of an incinerator on inorganic composition and lead isotope ratios of the atmospheric PM_{10}

Daniele Ziegler[1], Mery Malandrino[2*], Claudia Barolo[2], Gianpiero Adami[3], Milena Sacco[4], Francesco Pitasi[4], Ornella Abollino[5], Agnese Giacomino[5]

[1] Department of Applied Science and Technology, Polytechnic of Turin, Torino I-10129, Italy

[2] Department of Chemistry, NIS Interdepartmental and INSTM Reference Centre, University of Turin, Torino I-10125, Italy

[3] Department of Chemical and Pharmaceutical Sciences, University of Trieste, Trieste I-34127, Italy

[4] Piedmont Regional Agency for the Environmental Protection, Torino I-10135, Italy

[5] Department of Drug Science and Technology, University of Turin, University of Turin, Torino I-10125, Italy

Corresponding author. Mery Malandrino Via P. Giuria 5, 10125 Torino Italy.

E-mail address: mery.malandrino@unito.it (M. Malandrino).

Abstract:

A municipal solid waste incinerator (MSWI) was installed in a peripheral area of the city of Turin. In this study, we evaluated the contribution of this plant to the massive concentration of PM_{10}, to its chemical composition and to the distribution of the lead isotopes during the start-up phase.

We assessed the inorganic composition of PM_{10} collected in the vicinity of the Turin incinerator by inductively coupled plasma atomic emission spectroscopy (ICP-AES), magnetic sector inductively coupled plasma mass spectrometer (SF-ICP-MS) and ion chromatography (IC). The lead isotope ratios in PM_{10} samples were determined by SF-ICP-MS by a method developed and optimized using experimental design approach.

Element trends and data chemometric treatment evidence that the vehicular traffic, increased in this area due to the opening of the MSWI plant, and, to a lesser degree, the direct incinerator emissions influence As, Cd, Cr, Cu, Ba, Mo, Pb, Sn and Zn concentrations. As a whole, however, the element concentrations in PM_{10} and the Enrichment Factors (EFs) were comparable with the values reported for other urban sites and target pollutant concentrations of MSWI emissions, namely Cd, Cr, Cu and Pb, were lower than in PM_{10} emitted from older MSWIs. This confirms that incinerators of new installation have a lower impact on atmospheric PM_{10} composition thanks to stricter current legislation and up-to-date technologies. The lead isotope ratios investigation allowed to distinguish the diverse sources (crustal, vehicular traffic and MSWI) that influence lead concentration in PM_{10} collected near incinerator during start-up phase.

Keywords:

Incinerator; Trace elements in PM_{10}; Chemometric processing; Lead isotope ratios

List of Abbreviations

MSWI	Municipal Solid Waste Incinerator

IC	Ion Chromatography
ICP-AES	Inductively Coupled Plasma Atomic Emission Spectroscopy
SF-ICP-MS	Magnetic Sector Inductively Coupled Plasma Mass Spectrometer
EFs	Enrichment Factors
PM	Particulate Matter
WSI	Water Soluble Ions
TRM	Trattamento di Rifiuti Metropolitani
PCA	Principal Component Analysis
HCA	Hierarchical Cluster Analysis
CCD	Central Composite Design
PLS	Partial Least Square
PBL	Planetary Boundary Layer

1. Introduction

Air pollution represents one of the greatest concerns of urban environments. During the last decades great attention was paid to Particulate Matter (PM), due to the correlation between fine PM exposure and adverse health effects. The damage to health correlated to PM air pollution is one of the main environmental issues raised by World Health Organization.

The Po Valley covers the territory of several regions in Northern Italy and includes many urban agglomerates, such as Turin, Milan, Venice and Bologna. The area is densely populated and heavily industrialized. High amounts of atmospheric pollutants, e.g. about 400.000 tons of NO_x, 80.000 tons of PM and 250.000 tons of NH_3 (ammonia), are emitted per year by a wide variety of pollution sources, which are mainly related to traffic, domestic heating, industry and energy production, agriculture and farming activities (Raffaelli et al., 2020). Furthermore, the geographic conformation prevents an efficient dispersion of primary pollutants and causes a consequent high formation of secondary pollutants. The European

Environmental Agency indicated the Po Valley as a hot spot region for air pollutants, in particular for NO_2 in 2013 (EEA, 2013 and 2015).

The mechanisms responsible for the biological effects of particulate matter have been continuously undergone review, and many questions are still open about some relevant aspects, for example size fraction, number or mass of the particles, chemical components, among which metal elements are relevant species. Metals generally occur as different chemical compounds and in different oxidation states and are distributed among various dimensional fractions of the PM in the troposphere. Transport and distribution of aerosol particles strictly depend on their size, as well as to the weather conditions (Poschl, 2005).

Concentration, composition and size distribution of atmospheric particles are temporally and spatially highly variable. Altogether, however, particles size depends primarily on emission sources, and typically those emitted from anthropogenic sources are smaller than those emitted from natural ones (Harrison et al., 2012).

On the base of existing scientific evidence, many metals (often depending on their oxidation state) may have a direct or indirect active role in PM biological mechanisms of action.

Municipal solid waste incinerators (MSWIs) can be significant sources of atmospheric environmental pollution, potentially exposing nearby populations to hazardous chemicals at toxic levels. Both inorganic and organic chemicals have been identified in MSWI emissions, for instance carbon monoxide (CO), carbon dioxide (CO_2), sulphur oxides (SO_X), nitrogen oxides (NO_X), dioxins and furans, volatile organic compounds (VOC), polycyclic aromatic hydrocarbons (PAHs), metals and particulate matter (PM) (WHO, 2007). Some of these chemicals have been classified as known (group 1) or probable (group 2A) carcinogens for humans according to the International Agency for Research on Cancer (IARC, 2012). Some studies have suggested associations between MSWI emissions and health effects, particularly adverse impacts on reproduction and cancer (Vinceti et al., 2008).

Because of these troubles that have been identified in earlier studies, more recent investigations have been designed and implemented with the goal of establishing a better definition of exposure and/or effects arising from MSWIs.

Directive 2000/76/EC of the European Parliament and the Council on Incineration of Waste enforces measures to prevent or reduce negative effects to the environment, particularly emissions into air, soil and surface water, as well as to human health, which might arise from incineration and co-incineration of waste. More in detail, this directive states that incineration facilities shall be submitted to a permission to operate, which sets rigorous operating conditions, technical requirements and daily emission limits of 10 mg/m^3 for total dust and 0.5 mg/m^3 for the sum of Sb, As, Pb, Cr, Co, Cu, Mn, Ni and V (Directive 2000/76/EC, 2010). When discussing the environmental characteristics of a specific region, the identification of various sources of a pollutant becomes significant; consequently, the MSWI presence must be considered as a possible source of pollutants in airborne particulate matter. The knowledge of the metal content in PM is also important in recognizing its sources since these emit airborne PM with different metal distribution. MSWIs, indeed, play an important role in the treatment of municipal waste according to the recent European directives and it is very important to know the contribution of a MSWI plant of new generation to the inorganic composition of atmospheric PM_{10}. Many studies have evaluated the impact of MSWIs on air quality (Carignan et al., 2005; Pacyna et al.,2007; Font et al.,2015; Panepinto et al., 2018; Lucarelli et al., 2019) but, to our knowledge, none of these has evaluated the contribution during start-up phase.

Pb is a poisonous metal that can damage nervous connections especially in young children and cause blood and brain disorders (Tong et al., 2000; Gerhardsson, 2004; Meyer et al., 2008). The concentration of this heavy metal in PM is regulated by the Directive 2008/50/EC, which establishes a limit value of 0.5 μg/m^3 for a calendar year (Directive 2008/50/EC, 2008). Although lead occurs naturally in the environment, most of the high levels found throughout the environment derived from human activities. The European Union established the 1st of January 2000, as a limit date to remove leaded fuel from the market, although the European Commission conceded derogation to Spain, Italy and Greece until the 1st of January 2002. That is the reason why the concentration of this element in air has been decreasing since then, although other anthropogenic sources persist, such as smelting, steel mills, incineration of residues, wood and coal combustion, resuspension of contaminated soil dust and industrial activities (production of paintings, chemical agents, welds, etc.) (Widory et al., 2004, 2010; Zhao et al., 2017, 2019; Xu et al., 2020). The identification of stable lead isotope composition in atmospheric particulate matter of several cities around the world is being increasingly used to better characterize atmospheric lead sources (Carignan et al., 2005; Komarek et al., 2008; Guéguen et al., 2012; Gioia et al., 2010, 2017; Zhao et al. 2019; Lee et al., 2019; Xu et al., 2020).

This study focuses on:

- evaluation of the contribution of a new MSWI plant in start-up phase to total PM_{10} and its chemical composition in water soluble ions (WSI) and major, minor and trace elements;
- development, thorough an Experimental Design approach, of an accurate method for the calculation of lead isotope ratios using microwave acid digestion followed by magnetic sector inductively coupled plasma mass spectrometer (SF-ICP-MS) determination;
- discrimination between different sources of lead, known to be a marker of incinerator’s emission, through a study of its isotope ratios.

2. Materials and methods

2.1 Sampling location and PM_{10} collection

An incinerator was built in the city of Turin, a metropolitan area characterized by many industrial activities and huge volume of vehicular traffic, between 2010 and 2013 and initially was authorized to receive a maximum of 421,000 tons of waste per year from the province of Turin and from other regions. In July 2015, following revision of the Integrated Environmental Authorization, the plant's capacity was stepped up to 490,000 tons per year. This plant is precisely located in the south-western zone of Turin outskirts. It converts municipal solid waste, as well as special waste that can be combined with the municipal waste (up to a maximum of 124,000 tons per year), into electrical and thermal energy. More in detail, it consists in a moving grate with four methane burners able to produce 41 MW of electrical power and 106 MW of district heating simultaneously. It is managed by a metropolitan waste treatment society (Trattamento di Rifiuti

Metropolitani – TRM S.p.A.); for this reason, the sampling location is hereinafter referred to as TRM (http://trm.to.it/).

PM_{10} sampling was carried out in spring and summer 2013 in one site localized near the incinerator, in the area with the highest probability that PM emitted from the plant is falling to the ground. Air quality monitoring station is placed at 45°02'45" N and 7°37'00" E, in the Aldo Mei park of Beinasco town (Province of Turin) and it is managed by Regional Agency for Environmental Protection (ARPA, Piedmont). It is equipped with several instruments (PM_{10} and $PM_{2.5}$ Beta Attenuation Mass Monitor, Swam 5A Dual Channel model, FAI instruments; Analyzer for Nitrogen Compounds, 200E model, Teledyne API; PM_{10} Sampler, with a Sentinel 96 module for the automatic sequential sampling, Charlie model, TCR Tecora; dioxins/furans Sampler, ECHO HiVol model, TCR Tecora; Wet&Dry Deposimeter Samplers for dioxins/furans and polycyclic aromatic hydrocarbons, Labservice Analytica; Air Mercury Monitor, RA-915 AM model, Lumex) to detect specific air pollutants like NO_x, gaseous Hg, PM_{10} and $PM_{2.5}$ mass concentrations. A map of the metropolitan area, showing the position of the incinerator and the monitoring station, is reported in Figure 1.

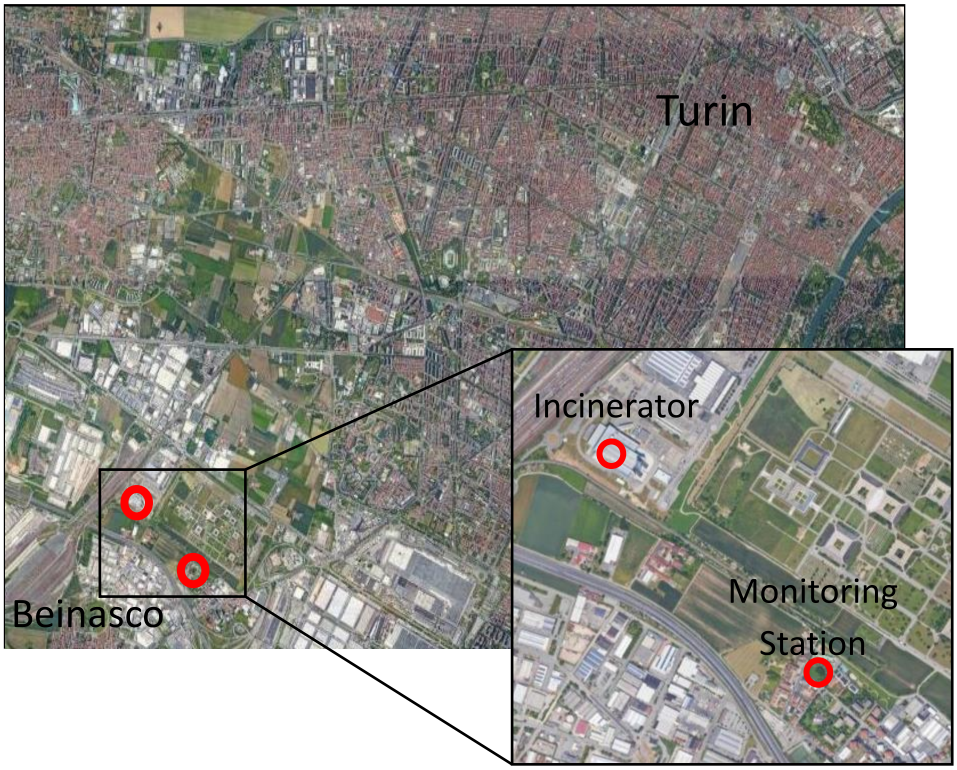
Turin
Incinerator
Monitoring Station
Beinasco

Figure 1: Geographical map of Piedmont and detail of the position of the incinerator and the monitoring station.

The PM_{10} samples were collected using a high-volume air sampler (Digitel DHA) and 80 and 150 mm diameter quartz filters to ensure a large amount of PM_{10} that would allow also the lead isotopic investigation. Sampling duration for each sample was fixed at 24 hours, at a flow of 29 m^3/h for a total volume of sampled air of 700 m^3.

A low volume air sampler, at a flow rate of 2.3 m^3/h and equipped with 47 mm diameter quartz filter, was adopted in order to evaluate daily mass concentration of PM_{10}. The flow control was carried out in the actual condition mode and the mass concentrations of PM_{10} were measured by weighing each filter before and after sampling on an analytical balance in a controlled atmosphere (20 °C, 50% relative humidity) according to Ministerial Decree 60/2002 (D.Lgs. 60, 2002). Meteorological conditions (i.e. average and maximum wind speed, average and maximum mixing height, and average temperature) were obtained from the Minerve calculation model, a diagnostic model for the reconstruction of three-dimensional wind and temperature fields (Table 1S Supplementary Material).

2.2 Choice of PM10 samples

The activity of Turin MSWI plant started on 19th April 2013, by testing the first combustion line. Then, from 22 May to 5 June also the second combustion line began to be active. Subsequently, from 5 June, the second combustion line of the plant was suspended, and it started again the activity in July.

Twenty-two samples were chosen for this study in the period between May and July 2013. The choice was performed considering the most representative days, based on the evaluation of two statistical methods: Principal Component Analysis (PCA) and Hierarchical Clustering Analysis (HCA) (shown in figure 1S, 2S and 3S in Supplementary Material).

Both meteorological parameters, obtained by a weather station located in the site, such as average and maximum wind speed (m/s), average temperature, average and maximum mixing height, and chemical parameters, such as PM_{10}, $PM_{2.5}$, NO_2 and NO concentrations (Table 1S), were considered, obtaining a dataset composed by 56 samples and 9 variables. These data were supplied by ARPA Piedmont.

All chemometric elaborations were carried out after autoscaling of the data. PC1 and PC2 collect the 62.6% (41.6% and 21% respectively) of total variance.

More in detail, from loading plot it was clear that both PM_{10} and $PM_{2.5}$ amounts are anticorrelated with wind speed, as expected; as a matter of fact, the samples collected in May are characterized by negative scores values on PC1, suggesting that these samples are most influenced by wind speed variable. This is true especially for samples 25 and 26 May (25/5 and 26/5), two weekend days, when the airborne particulate emitted by tracks is consistently reduced; these samples, together with 29 May (29/5) and 31 May (31/5), show the minimum amount of PM_{10} and, in the score plot, are placed in opposite position to the vector representing this variable.

In fact, during May, higher speed of wind values was recorded, resulting in an enhanced dispersion of particulate matter respect to the summer period. Surprisingly, temperature variable is quite correlated to PM_{10} amount in troposphere. This phenomenon can be due to the enhanced rainfall recorded in May, resulting in a decrease of both temperature and coarse fraction of particulate matter. Moreover, NO concentration appears anti-correlated with mixing height. NO presence has an influence in the concentration of NO_2, that is obtained from the former after a photochemical oxidation in troposphere due to ozone. In the month of May, NO concentration is higher than in June and July, due to the lower height of the PBL (Planetary Boundary Layer). Finally, PM_{10} and $PM_{2.5}$ concentrations are correlated with NO_2 concentration, and they are also anti-correlated with the wind speed as seen in Yadav et al. (2014), describing a more polluted environment for higher PM and NO_2 concentrations. This phenomenon is verified especially for three weekdays, 17, 18 and 19 June (17/6, 18/6 and 19/6), in which samples are characterized by PM_{10} concentrations up to 30 $\mu g/m^3$ with a reduced transport of particulate matter over long distances.

In addition, through HCA three main clusters were detected: a cluster composed by the samples collected at the end of May, displaying lower PM_{10} concentrations and other two clusters comprising the samples from June and July separated according to PM_{10} concentrations and the weather conditions.

We chose PM_{10} samples considering the results obtained from both chemometric techniques: PM_{10} samples more influenced by PC1 and PC2 and representing evenly the clusters evidenced by HCA were selected. PM_{10} samples having the highest and the lowest PM_{10} concentration in each month were also selected. Our selection criterion has permitted us to compare days with a high and a low concentration of particulate matter and to provide information on the dominant sources of atmospheric aerosol in the investigated area, even if we cannot consider this selection as representative of the possible patterns of atmospheric pollutants in the whole period.

2.2 Element and WSI determination

All filters have been analyzed to determine the mass of particulate collected using a gravimetric technique according to Ministerial Decree 155/ 2010 (D.Lgs. 155, 2010).

The aerosol-loaded filters (143 mm of the total 150 mm diameter) were punched into 36 mm diameter circular sections. The determination of elements and WSI was executed in duplicate and, for each replicate, two aliquots of each filter were considered. This approach showed that PM_{10} distribution on filters was equable. In fact, relative standard deviation (RSD) was <10% for all the elements except for potassium with a value equal to 15%.

Each sub-sample for element determination was digested by a microwave oven (Milestone-Ethos One) with a mixture of 3.5 mL of sub-boiled HNO_3, 1.5 mL of ultra-pure H_2O_2 (Sigma-Aldrich) and 3 mL of HPW (Milli-Q (Millipore) ultrapure water, resistivity = 18.2 MΩ cm) in 100 mL tetrafluoromethoxyl vessels. The following heating steps were applied: 5 min ramp until 170 °C, 10 min dwell at 170 °C, 5 min ramp until 200 °C, 20 min dwell at 200 °C, and 30 min of ventilation. The resulting solutions were filtered on cellulose filters (Whatman Grade 5) to eliminate the undissolved filter parts and diluted to 30 mL with HPW. By this method, the concentrations of trace elements not enclosed in silicate matrix were transferred quantitatively into solution.

Elements present in lower concentrations were determined by SF-ICP-MS (Thermo Finnigan Element 2). Mass resolution and isotope selection were optimized for each element to ensure resolution of spectral interferences and maximize sensitivity. The following isotopes of the investigated elements were monitored: ^{47}Ti, ^{48}Ti, ^{51}V, ^{53}Cr, ^{63}Cu, ^{65}Cu, ^{68}Zn, ^{75}As, ^{90}Zr, ^{95}Mo, ^{98}Mo, ^{111}Cd, ^{112}Cd, ^{114}Cd, ^{118}Sn, ^{138}Ba, ^{207}Pb, ^{208}Pb at low resolution (R=400); ^{46}Ti, ^{59}Co, ^{60}Ni, ^{61}Ni, ^{62}Ni, ^{64}Zn, ^{66}Zn, ^{96}Mo, ^{113}Cd, ^{139}La, ^{140}Ce, ^{203}Tl, ^{205}Tl, ^{204}Pb, ^{206}Pb at medium resolution (R=4,000). Analyses on each sample were conducted following a 60s uptake and stabilization period. In low resolution 9 replications (3 run x 3 passes) for each selected isotope were carried out, while in medium resolution 12 replications (4 run x 3 passes) for every isotope were carried out. Between samples the nebulizer system was rinsed for 2 min with 2% sub-boiled HNO_3, which eliminated carry-over and reconditioned the sampler cone. Power applied was 1270 W, 1 L/min flow of both auxiliary and nebulizer gasses, while plasma gas was fluxed at 16 L/min.

The following elements: Ca, Al, Na, K, Mg, Mn and Fe present in higher concentrations in PM samples, were determined by Inductively Coupled Plasma Atomic Emission Spectroscopy, ICP-AES (Perkin Elmer, model Optima 7000 DV).

The power applied was 1300 W. Plasma, auxiliary and nebulizer gas flows were 15, 0.2 and 0.6 L/min respectively. The signals were measured in triplicate.

Sets of instrumental blank and calibration verification checks were run at frequent intervals during the batch sequences for both SF-ICP-MS and ICP-AES analyses. The calibrations were performed with standard solutions prepared in aliquots of process blanks. Process blanks were incorporated into the dissolution and analytical procedure to assess metal contribution from the filters, bombs, Milli-Q water and purified acids used in this procedure. Limits of detection (LODs), corresponding to three times the standard deviation of the reagent blank, were experimentally determined by ICP-AES and SF-ICP-MS and are respectively reported in Table 2S and 3S (Supplementary Material).

All the elements investigated, namely Al, As, Ba, Ca, Cd, Ce, Co, Cr, Cu, Fe, K, La, Mg, Mn, Mo, Na, Ni, Pb, Sn, Ti, Tl, V, Zn and Zr, are commonly used, with the aid of chemometric treatments and other graphical and mathematical tools, as chemical markers for identifying the anthropogenic and natural (crustal and marine) sources of atmospheric PM.

Sampling was carried out over three months, namely May-July 2013, using two distinct types of filters: Millipore© for the first month and Munktell for the remaining time. The sample blank values were measured for each filter type and all the sample signals were subtracted of their appropriate sample blank values. Sample blank concentrations (µg/L or ng/L) are reported in Table 2S and 3S.

NIST SRM 1648a (Urban Particulate Matter) and NIES CRM 8 (Vehicle Exhaust Particulates) were used for evaluating the procedural recoveries and for identifying the best analytical parameters. Most of the relative errors for the analytes are lower than 10%, except for some elements of geogenic origin like Al, La, Ce and Ti, which are unlikely to be completely extracted without HF.

Finally, the WSI concentrations were determined using an Ion Chromatography (IC) system (Dionex, DX-100, configuration DX 500 for anions and configuration DX 320 for cations). Four circular filter sections (36 mm diameter) for two replicates were placed in 10 mL of HPW and sonicated for 30 minutes to obtain an extraction solution, which was then filtered using a 0.22 µm pore syringe filter. The anion (NO_3^-, Cl^- and SO_4^{2-}) concentrations were measured using an AS11-HC column (4 x 250 mm) with 30 mM KOH while the cation (NH_4^+, Na^+, K^+, Mg^{2+} and Ca^{2+}) concentrations were determined using an Ion Pac CS12A column (4 x 250 mm) with 20 mM methanesulfonic acid as an eluent at a flow rate of 1.0 mL/min. LOD and sample blank concentrations for WSI are reported in Table 4S (Supplementary Material).

2.3 Statistic Data Analysis

The chemometric treatment was carried out using XlStat 2017 software package, an add-on of Microsoft Excel. PCA is a statistical method that uses an orthogonal conversion of a group of observations of possibly correlated variables into a set of uncorrelated variables, obtained by linear combination of the original ones, called principal components (PCs). The number of PCs is less than or equal to the number of original variables. The first principal component has the largest possible variance and the resulting vectors are an uncorrelated orthogonal basis set (Cohen et al., 2003). HCA is a method of group analysis which explores the dataset to build a hierarchy of clusters. An agglomerative procedure was used for clustering: this is a "bottom up" approach, in which each observation starts in its own cluster, and pairs of clusters are merged as one moves up the hierarchy (Rokach and Maimon, 2005). For performing PCA and HCA, the whole dataset was autoscaled. Finally, Kruskal-Wallis test (significance level: 95% and 90%) was performed for checking if the analyte concentrations determined in PM_{10} samples collected in 2012, 2013 and 2014 in TRM monitoring station were significantly different. The same non-parametric test was used to evaluate if As, Cd, Ni and Pb concentrations in PM_{10} samples collected in Druento, Torino-Consolata and TRM monitoring stations in 2013 and in May, June and July months in 2014-2018 years were significantly different.

2.3 SRM-Lead isotope ratios analysis

The evaluation of lead isotopic ratios was carried out by SF-ICP-MS considering two circular filter sections of 36 mm of diameter. These sections were punched using an INOX punch: in this way, an enhanced accuracy is guaranteed compared to dividing the filter in four parts using clippers. In fact, the relative standard deviations of replicates were always lower than 10%.

In order to evaluate lead isotope ratios, a NIST SRM 981 (Common lead isotopic standard) was used. This certified standard reflects the natural abundance of four lead isotopes: 204 (1.4255 ± 0.0012%), 206 (24.1442 ± 0.0057%), 207 (22.0833 ± 0.0027%), 208 (52.347 ± 0.0086%).

SRM 981 was utilized for correcting the bias introduced by instrumental mass discrimination. A solution containing 1.2 mg/L of lead in 0.05% ultrapure nitric acid matrix was prepared for that objective. The values used for the mass bias correction were 0.059042 ± 0.000037, 0.91464 ± 0.00033, 2.1681 ± 0.0008 respectively for 204/206, 207/206 and 208/206 ratio, as reported on the certificate released by NIST, with errors calculated at 95% confidence interval.

A Central Composite Design (CCD) with a total of 27 experiments was chosen to optimize the following instrumental parameters was carried out:

- Integration window (window of masses to integrate peaks)
- Sampling points per peak (number of points counted in the window of masses chosen)

- Integration times (runs x passes), equal to the replications.

The ranges used for these parameters were 60-100%, 5-30 and from 1x1 to 9x9 respectively. These ranges were applied also by Zhu et al. (2006).

After evaluating lead concentration in samples analyzed, the concentrations of 2.5 µg/L and 25 µg/L of lead in SRM 981 were chosen, respectively equal to the minimum and the maximum Pb concentration in the samples. In addition, all the measurements were carried out working in both low and medium resolution.

In this work, the number of factors *(k)* is equal to 4 (integration window, sampling points per peak, runs and passes) and 2 levels *(L)* for each factor were assigned (minimum and maximum value of above reported ranges). Experiments to be realized are equal to $L^k + L*k+n$, where n is the number of the central points (three in this case) (Lundstedt et al., 1998). This chemometric approach was carried out within the software Modde 9.1 (https://umetrics.com/product/modde).

3. Results and discussion

3.1 Chemical composition

3.1.1 Mass and element concentrations

The PM_{10} and element concentrations (mean, standard deviation, and 5th - 95th percentiles) for each month (May, June and July) are reported in Table 1 while PM_{10} and element concentrations (mean and standard deviation) in each PM_{10} sample are shown in Tables 5S, 6S and 7S (Supplementary Material).

Table 1. Mean and standard deviation (Mean ± SD), and 5th - 95th percentiles of each element determined in PM_{10} samples and PM_{10} massive concentration, divided by month. All values, except for PM_{10}, are expressed in ng/m^3. PM_{10} is expressed in µg/m^3.

	May		**June**		**July**	
Element	**Mean ± SD**	**5th - 95th perc.**	**Mean ± SD**	**5th - 95th perc.**	**Mean ± SD**	**5th - 95th perc.**
PM_{10}	9 ± 5	5 - 17	31 ± 4	24 - 35	23 ± 3	20 - 27
Al	155 ± 63	90 - 228	477 ± 205	207 - 688	326 ± 137	171 - 522
As	0.61 ± 0.05	0.55 - 0.68	0.80 ± 0.31	0.46 - 1.23	0.41 ± 0.09	0.30 - 0.54
Ba	6.05 ± 1.34	4.50 - 7.93	30.0 ± 25.0	7.05 - 61.6	35.1 ± 16.7	12.9 - 49.9
Ca	235 ± 96	140 - 350	575 ± 208	296 -808	354 ± 139	186 - 530
Cd	0.05 ± 0.04	0.03 - 0.11	0.08 ± 0.02	0.06 - 0.11	0.08 ± 0.01	0.06 - 0.09
Ce	0.16 ± 0.07	0.08 - 0.25	0.46 ± 0.23	0.14 - 0.73	0.21 ± 0.15	0.08 - 0.42
Co	0.08 ± 0.06	0.03 - 0.16	0.28 ± 0.35	0.06 - 0.81	0.10 ± 0.04	0.05 - 0.15
Cr	0.67 ± 0.57	0.07 - 1.26	3.83 ± 2.43	0.64 - 6.63	3.29 ± 1.19	1.63 - 4.63
Cu	9.39 ± 1.58	7.37 - 11.4	18.6 ± 3.80	12.8 - 22.4	14.3 ± 3.83	9.73 - 19.8
Fe	288 ± 66	210 ± 365	631 ± 207	347 - 848	440 ± 161	251 - 675
K	81.9 ± 39.3	39 - 133	251 ± 69	157 - 318	187 ± 52	140 - 266
La	0.10 ± 0.04	0.06 - 0.16	0.35 ± 0.15	0.14 - 0.53	0.21 ± 0.10	0.11 - 0.37
Mg	142 ± 80	75 - 254	307 ± 128	137 - 445	204 ± 89	101 - 328
Mn	6.30 ± 1.26	5.33 - 8.25	24.4 ± 8.7	12.6 - 33.8	14.3 ± 5.4	8.51 - 21.1
Mo	0.32 ± 0.11	0.19 - 0.46	0.82 ± 0.19	0.55 - 1.02	0.67 ± 0.17	0.45 - 0.89
Na	302 ± 365	18 - 775	137 ± 28	96 - 165	76.6 ± 34	35 - 117
Ni	1.56 ± 0.66	0.89 - 2.45	3.86 ± 0.92	2.63 - 4.89	2.37 ± 0.74	1.59 - 3.48
Pb	1.17 ± 0.63	0.60 - 2.11	4.81 ± 1.58	2.88 - 6.98	3.16 ± 0.74	2.30 - 4.15
Sn	2.91 ± 0.80	1.77 - 3.73	5.38 ± 0.91	4.20 - 6.43	3.96 ± 0.90	2.79 - 5.20
Ti	5.29 ± 1.65	3.54 - 7.17	14.5 ± 6.55	6.13 - 21.7	10.7 ± 4.10	5.96 - 16.4
Tl	0.004 ± 0.002	0.002 - 0.007	0.019 ± 0.005	0.013 - 0.025	0.013 ± 0.002	0.010 - 0.015
V	0.85 ± 0.81	0.24 - 2.10	3.14 ± 0.93	2.04 - 4.24	1.17 ± 0.37	0.71 - 1.62
Zn	14.5 ± 5.2	8.60 - 21.3	29.3 ± 13.5	13.0 - 47.0	24.5 ± 11.6	11.8 - 37.6
Zr	0.41 ± 0.13	0.29 - 0.61	0.85 ± 0.24	0.48 - 1.06	0.51 ± 0.17	0.30 - 0.76

Generally, PM_{10} concentrations are smaller in the month of May compared to June and July, as a consequence of an enhanced presence of winds at the ground resulting in longer ranges of dispersion of particulate matter.

Regarding metal concentrations in PM_{10}, the highest concentrations were found for the typically crustal elements, namely for Na, Al, Ca, Fe and Mg, clarifying the significant contribution of soil and re-suspended mineral particles to atmospheric PM, as reported in Padoan et al. (2016).

Considering the target values for As, Cd, Ni and the threshold value for Pb, reported in the European legislation (D. Lgs. 155, 2010), that are respectively 6, 5 and 20 ng/m^3 for the first three and 0.5 µg/m^3 for lead, it is notable that the concentrations of these analytes in all samples are one or two orders of magnitude lower than these values. These elements are the main targets for anthropogenic contributions, especially regarding combustion of fossil fuels and motor vehicles.

For trying to evaluate if the start-up phase of the incinerator resulted in an increase of the element concentrations in PM_{10}, the element concentration trends have been considered (Figure 2). Overall, on the basis of the concentration trends, elements could be divided into three groups. Group 1 elements (As, Co, Na and V) show higher concentrations in May and June; Group 2 elements (Al, Ba, Ca, Ce, Cu, Fe, La, Mn, Ni, Ti, Zn and Zr) show an increase in their concentrations in June and at the beginning of July followed by a decrease around the middle of July; the concentrations of Group 3 elements (Cd, Cr, K, Mo, Pb, Sn and Tl) increase between May and June and remain almost constant in July.

As and V, belonging to the Group 1, are often referred to be emitted by incinerator plants (Sakata et al., 2000; Font et al., 2015), Na, instead, might derive from $NaHCO_3$, used at the Turin incinerator plant for the abatement of acids from vapor emissions (http://trm.to.it/), the Co behavior is more difficult to explain because it is characterized by a very high concentration in 17 June sample but, to our knowledge, no particular event relating to the incinerator or, in general, to the air quality occurred on that date. It is noteworthy that from 22 May to 5 June the second combustion line was also put into operation for the first time and this could have led to the release of higher concentrations of Na and, to a lesser degree, As and V into the atmosphere.

Most of the elements belonging to the Group 2 are typically geogenic, precisely Al, Ca, Ce, La, Ti and Zr. The same trend is also shown by Ba, Cu, Fe, Mn and Zn commonly associated also with non-exhaust vehicle emissions, as they are common indicators of release by mechanical abrasion of metal structures of vehicles, engine components, brake and tires wear and road dust (Birmili et al., 2006; Councell et al., 2004; Amato, 2008). It is possible that between June and July, due to the start of the incinerator activities and the drier summer climate, proved also by the increase in temperatures recorded starting from mid-June, the road and soil dust resuspension phenomena are intensified, leading to enrichment of the typical elements of these sources in the PM_{10}. Finally, the elements included in Group 3 are typically emitted during several combustion and industrial production processes: in particular Cd, Cr, Pb and Sn are also commonly associated with incinerator emissions (Pacyna et al.,2007; Font et al.,2015).

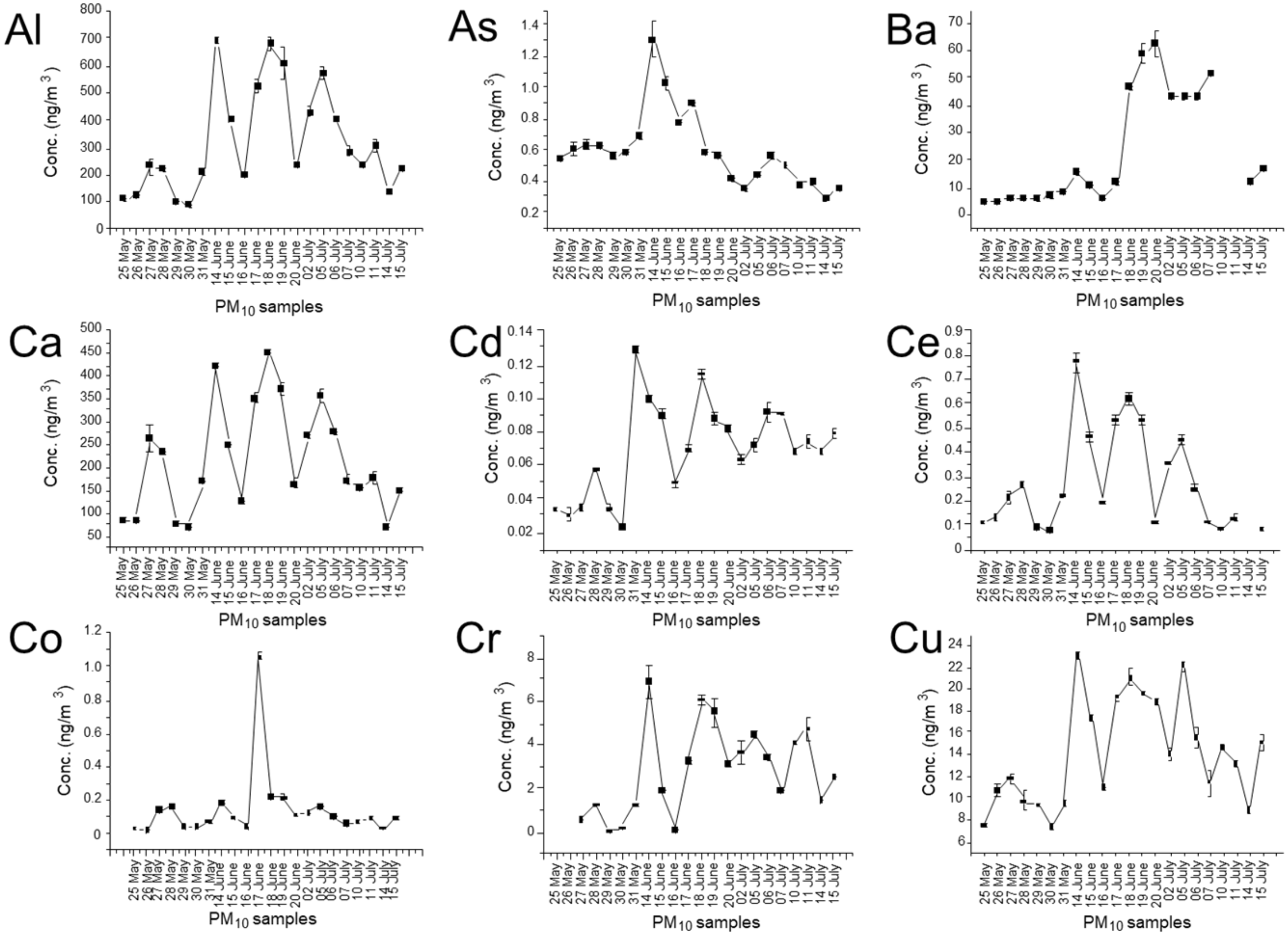
Al
As
Ba
Ca
Cd
Ce
Co
Cr
Cu
Conc. (ng/m 3)
PM10 samples
25 May
26 May
27 May
28 May
29 May
30 May
31 May
14 June
15 June
16 June
17 June
18 June
19 June
20 June
02 July
05 July
06 July
07 July
10 July
11 July
14 July
15 July

(continued)

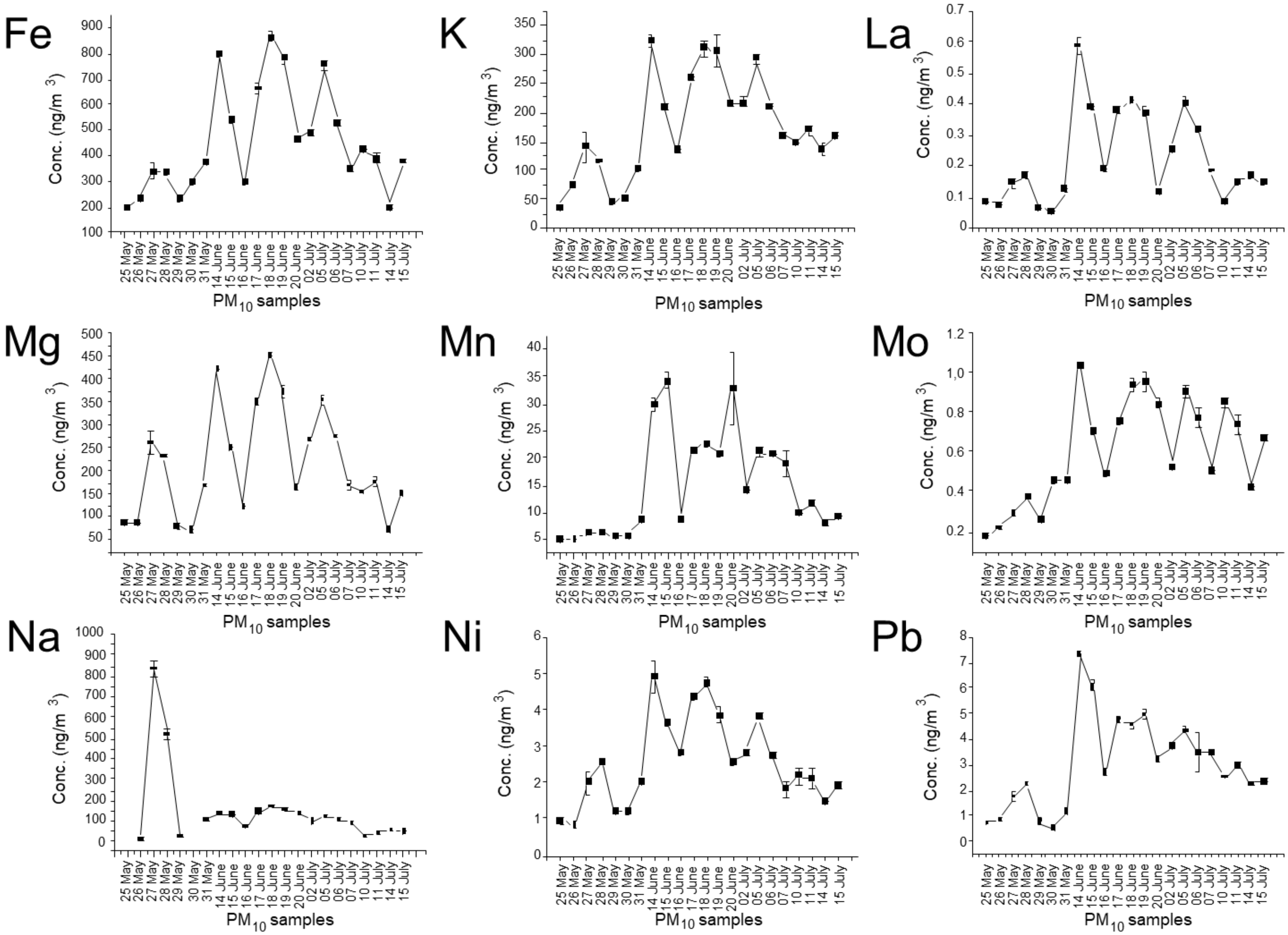
Fe
K
La
Mg
Mn
Mo
Na
Ni
Pb
Conc. (ng/m 3)
PM10 samples
25 May
26 May
27 May
28 May
29 May
30 May
31 May
14 June
15 June
16 June
17 June
18 June
19 June
20 June
02 July
05 July
06 July
07 July
10 July
11 July
14 July
15 July

(continued)

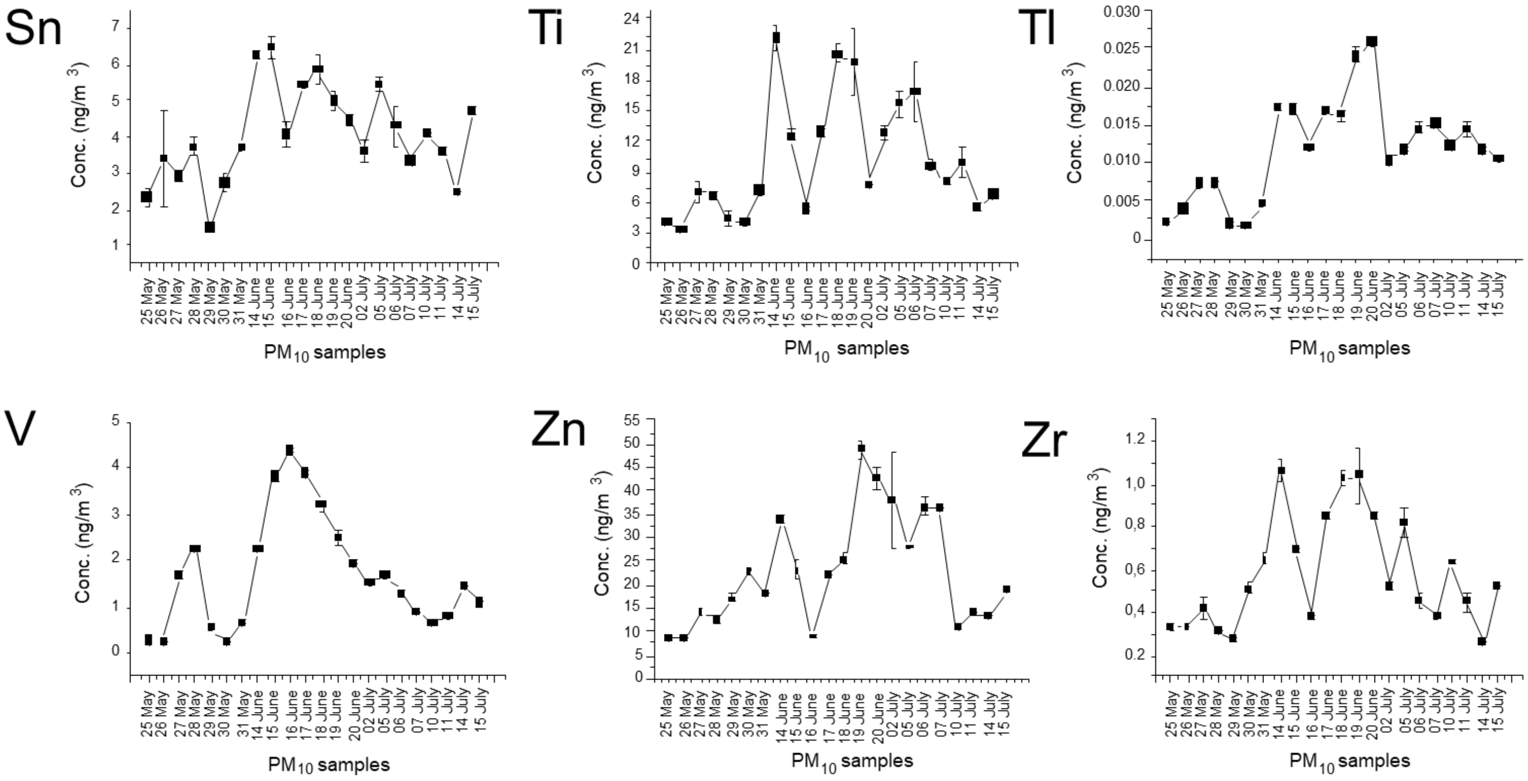
Sn
Ti
Tl
V
Zn
Zr
Conc. (ng/m 3)
PM10 samples
25 May
26 May
27 May
28 May
29 May
30 May
31 May
14 June
15 June
16 June
17 June
18 June
19 June
20 June
02 July
05 July
06 July
07 July
10 July
11 July
14 July
15 July
0.030
0.025
0.020
0.015
0.010
0.005
0
55
50
45
40
35
30
25
20
15
10
5
0
1.2
1,0
0,8
0,6
0,4
0.2

Figure 2: Element trends during start-up phase of the incinerator.

In an effort to gain insight into the possible sources of PM_{10}, a chemometric treatment of the experimental data was carried out through the well-known Q-mode HCA in which we assume that different levels of dissimilarity among elements are indicative of different emission sources (Figure 3).

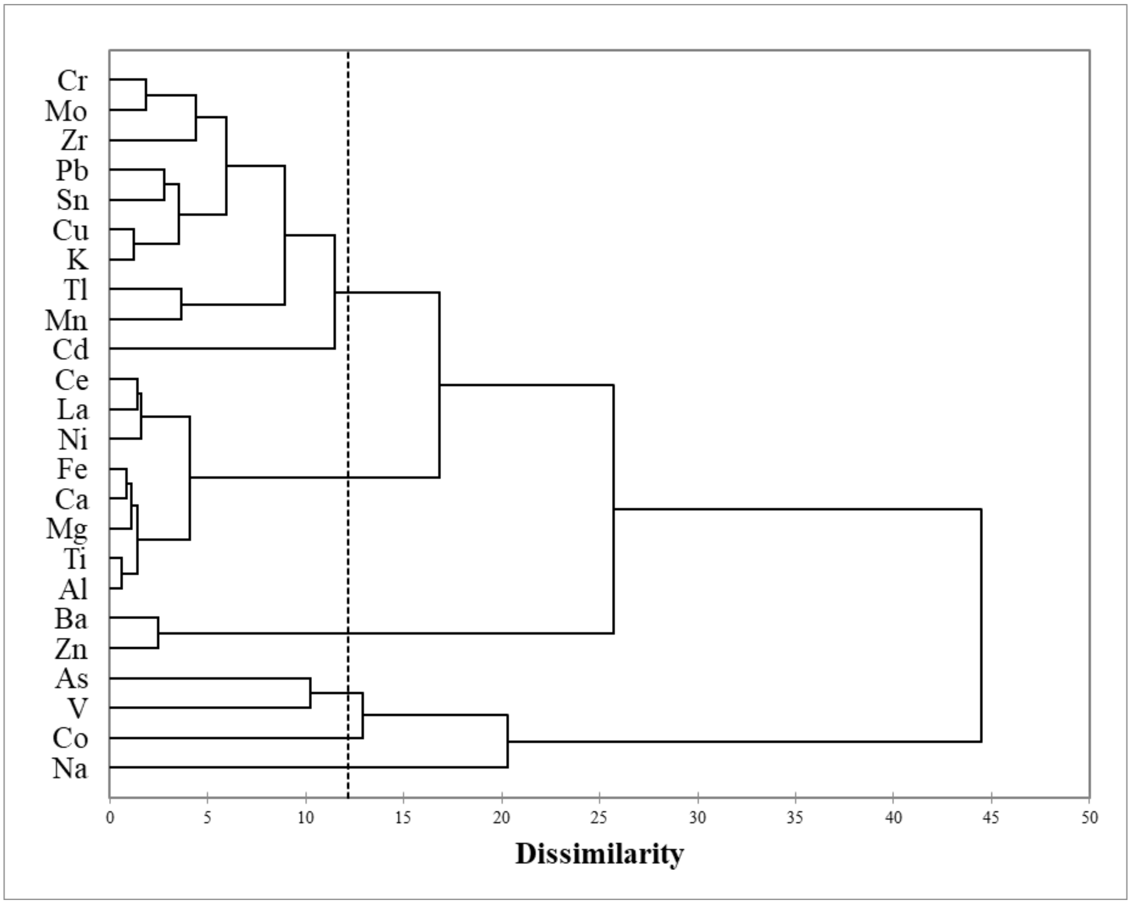

Figure 3: Dendrogram obtained by Q-mode HCA

Starting from the bottom of the figure, the first cluster is composed by As, Co, Na and V, i.e. the elements belonging to Group 1: they are linked at high levels of dissimilarity, suggesting that they do not derive from a single emission source but they are likely all emitted in atmosphere from several anthropogenic sources, probably attributable also to activities that have occurred in the start-up phase of the incinerator, such as the temporary commissioning of the second combustion line. A second cluster is characterized by only two elements, namely Ba and Zn; several researchers (Pakkanen et al., 2001; Malandrino et al. 2013; Zhang et al. 2020) identified these elements as typical markers of road dust source because the former is added to lubricating oils to prevent smoke and diesel engine abrasion and the latter is also generated by dust caused by vehicular movement or exhaust emission. It is necessary to specify that generally these elements are also associated with crustal elements in identifying the road dust source, while here they are linked at high level of dissimilarity with these elements grouped together in a third cluster. This could be due to the fact that while crustal elements are enriched when the environmental conditions are favorable to the resuspension of soil dust, the resuspension of road dust occurred due to the heavier traffic of trucks carrying the wastes to the incinerator. As already mentioned, the third cluster is characterized by several elements, namely Al, Ca, Ce, Fe, La, Mg, Ni and Ti, that are linked at low levels of dissimilarity, suggesting a common source associated with soil dust. Finally the last cluster groups many elements, namely K, Cr, Cu, Mn, Mo, Pb, Sn, Tl and Zr, that are linked at different levels of dissimilarity, suggesting that they are emitted in atmosphere from several anthropogenic sources. In particular, the clustering of K, Cu, Pb and Sn could represent the direct incinerator emissions since Pb, Sn and Cu are commonly associated with this source and K is a common marker of biomass burning events (Lucarelli et al., 2019) while the other elements probably derive from city vehicular traffic and other industrial activities.

Overall, it is likely that the increase of concentrations for Ba, Cd, Cr, Cu, K, Mo, Pb, Sn and Zn during start-up phase of MSWI plant was caused by a combination of factors: the vehicular traffic, presumably increased in this area due to the commissioning of the incinerator, and a possible direct contribution deriving from the incinerator emissions; however, a contribution from the city vehicular traffic and industrial activities cannot be excluded.

In this study, a comparison between results obtained in two nearby areas (Padoan et al., 2016) for an urban site (Torino-Consolata, TO-Consolata) and a rural site (Druento) in 2011 and in the same monitoring station between October and December in 2012 and 2014 was accomplished in order to identify a possible variation of PM sources and/or of their influence due to the MSWI start-up (Table 2). TO-Consolata site is localized in the historical centre of Turin and is mainly affected by vehicular traffic and heating emissions. Druento site is classified as a rural site by ARPA Piedmont and is localized in the small town of Druento, within a regional park, with no direct influence of urban activities. This station is considered as a background site. In Figure 4 it is possible to notice the difference between the three sites for twenty-one elements having high (a), intermediate (b) and low (c) concentrations.

Table 2. Mean and standard deviation (Mean ± SD), and 5th - 95th percentiles of each element determined in PM_{10} samples collected in TRM site in 2013. For comparison, descriptive statistics of the inorganic composition of the PM_{10} collected in TRM site in 2012 and 2014 (Conca et al., 2020) and in TO-Consolata and Druento sites in 2011 (Padoan et al., 2016) are also reported. All the concentrations are expressed in ng/m^3.

	This study		**2012 TRM**		**2014 TRM**		**2011 TO - Consolata**		**2011 Druento**	
	Mean ± SD	**5th - 95th perc.**	**Mean**	**5th - 95th perc.**	**Mean**	**5th - 95th perc.**	**Mean**	**Range**	**Mean**	**Range**
Al	319 ± 192	102 – 677	170	33 - 470	250	98 - 530	203	17.8 - 428	137	4.08 - 531
As	0.60 ± 0.24	0.35 – 1.02	0.48	0.059 - 1.7	1.1	0.26 - 2.9	0.71	0.18 - 1.48	0.38	0.14 – 0.7
Ba	23 ± 21	4.8 – 58.8	48	19 - 150	52	40 - 78	32.1	12.4 – 76.9	16.7	7.39 – 54.5
Ca	387 ± 203	139 – 780	580	140 - 1200	1700	840 - 5000	749	18.7 – 1517	482	146 – 1460
Cd	0.07 ± 0.03	0.03 – 0.11	0.32	0.12 - 0.83	0.29	0.020 - 2.7	0.62	0.19 - 1.08	0.31	0.05 – 1.01
Ce	0.28 ± 0.21	0.08 – 0.62	0.33	0.076 - 0.66	0.34	0.16 - 0.65	0.22	0 - 0.88	0.15	0 – 1.53
Co	0.15 ± 0.21	0.036 – 0.22	0.32	0.036 - 1.1	0.31	0.082 - 0.64	0.7	0.06 - 1.85	0.18	0 – 0.87
Cr	2.8 ± 2.0	0.09 – 6.08	6.4	2.4 - 12	5.2	2.3 - 12	8.24	1.9 – 14.3	5.22	0.51 – 12.5
Cu	14.1 ± 4.9	7.55 – 22.0	40	7.8 - 79	27	11 - 77	22.3	5.04 – 52.4	3.9	0 – 15.1
Fe	453 ± 204	203 – 800	1200	260 - 2200	720	230 - 1700	1316	272 - 3164	356	57.4 – 658
K	174 ± 87	46 – 309	360	61 - 1100	860	330 - 2100	486	79.4 - 1285	232	56.8 – 472
La	0.22 ± 0.14	0.065 – 0.41	0.19	0.076 - 0.34	0.12	0.060 - 0.34	< 0.007	<0.007	0.02	0 – 0.47
Mg	217 ± 117	74 – 421	190	44 - 460	290	170 - 600	254	19 - 738	148	6.77 – 314
Mn	15 ± 9	5.4 – 33	14	2.6 - 27	12	3.3 - 30	17.3	3.63 – 37.5	8.23	2.04 – 31.3
Mo	0.61 ± 0.26	0.22 – 0.96	3.4	1.6 - 7.3	3.4	1.1 - 7.3	4.86	0.83 – 16.02	1.09	0.24 – 3.03
Na	154 ± 192	27 – 538	136	29 – 360	758	172 – 2303	n.a.	n.a.	n.a.	n.a.
Ni	2.6 ± 1.2	0.96 – 4.8	4.1	0.58 - 9.3	7.7	2.9 - 25.3	5.74	0 – 16.2	6.45	0 – 41.9
Pb	3.0 ± 1.8	0.76 – 6.0	8.5	0 - 26	10	3.2 - 25	16.3	3.8 – 44.6	6.06	1.7 – 13.2
Ti	10 ± 6	4.0 – 20	19	1.9 - 51	16	5.0 - 34	23.5	2.29 – 54	18.5	4.99 – 33.7
V	1.7 ± 1.2	0.26 – 3.9	1.3	0.20 - 3.1	1.2	0.34 - 2.2	3.15	1.06 - 5.73	1.44	0.67 – 2.5
Zn	23 ± 12	8.7 – 42	68	19 - 160	130	45 - 390	64.3	19.6 - 164	37.9	4.81 – 79.3
Zr	0.58 ± 0.26	0.28 – 1.04	n.a.	n.a.	n.a.	n.a.	1.66	0.29 – 4.01	0.38	0 – 3.43

n.a.: not available

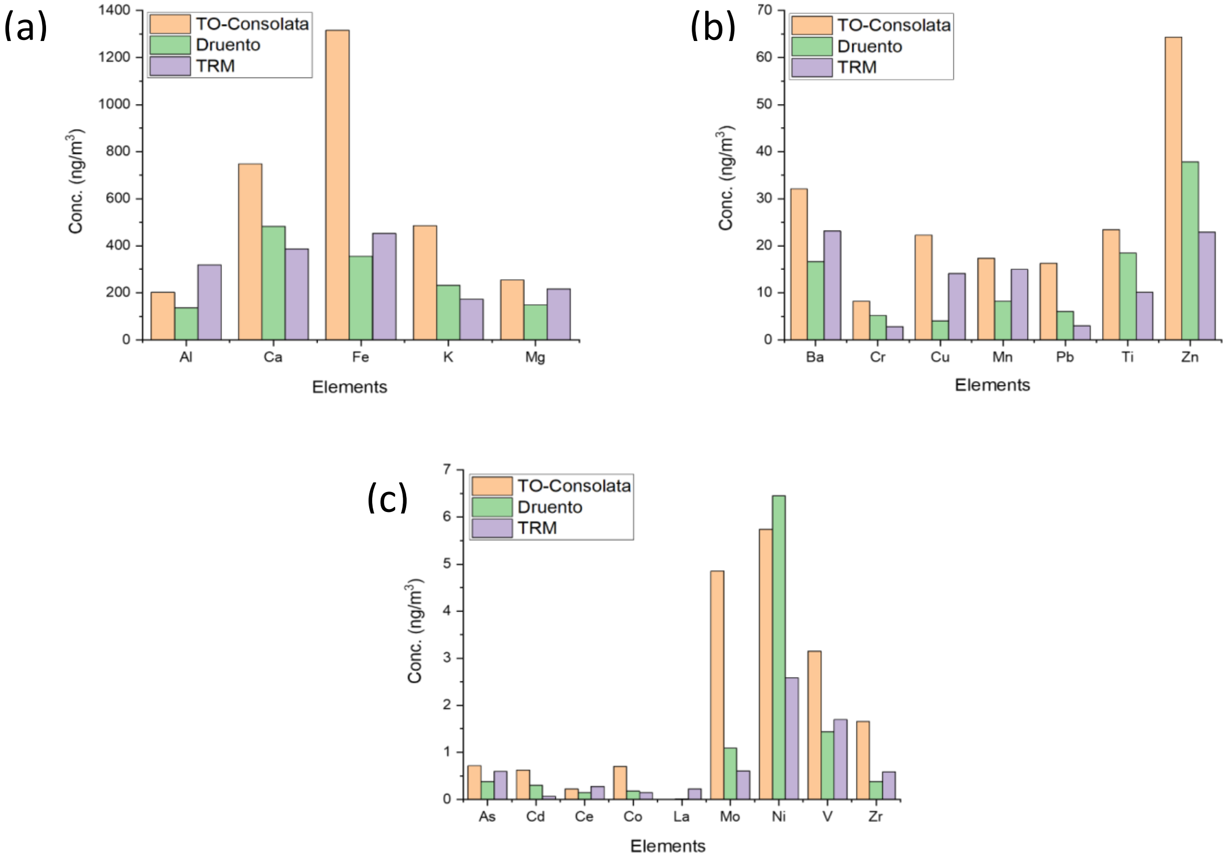

***Figure 4**: Concentrations of metals and metalloids in PM_{10} in TO-Consolata (urban), Druento (rural) and TRM (sub-urban) sites. (a) high, (b) intermediate and (c) low concentrations.*

Generally, the concentration of analytes in TRM site is in between with respect to the urban site and the rural one. In the urban site higher concentrations of analytes deriving from anthropogenic activities were measured, due to vehicular traffic and industrial and residential combustion processes.

On the other hand, Al, La and Ce concentrations are slightly higher in the TRM site than in the other two locations. Since the most probable common source for these elements is represented by the Earth's crust, their concentration is usually higher when soil dust resuspension events are more likely, that is when higher speed of wind is observed, as reported in May month in TRM site.

TRM site is considered a sub-urban site. Indeed, concentrations of these target metals are quite high compared to rural sites, but still they are comparable to other sub-urbans sites (Gholampour et al., 2016). Finally, the element concentrations in TRM site during start-up phase of the incinerator are comparable or lower than those found in PM_{10} samples collected in the same monitoring station in 2012 and 2013. This mainly happens due to the frequent thermal inversions occurring during autumn and winter. These climatic phenomena have a relevant effect, particularly in orographically complex areas such as the Alpine arc surrounding the North-West sector of Piedmont. The stagnation of air in the valley floors, caused by severe thermal inversions in winter, gives rise to an accumulation of all pollutants. In some situations, when the thermal inversion is very strong while the foehn winds are weak, air recirculation is limited, resulting in intense urban pollution. These results underline the unquestionable role of meteorology in the evolution of pollutant concentrations in air and the overall low contribution of elements arising from MSWI plant also during the start-up phase.

Finally, in Table 3, we compare the total $PM_{10,}$ As, Cd, Ni and Pb concentrations found in PM_{10} samples collected in Torino Consolata, Druento and TRM sites in all 2013 and in May – July quarters of 2014-2018. It is evident that the concentrations for these elements in TRM site are in between the other two sites (ARPA Piemonte, 2013a; ARPA Piemonte, 2013b; ARPA Piemonte, 2014; ARPA Piemonte, 2015; ARPA Piemonte, 2016; ARPA Piemonte, 2017; ARPA Piemonte, 2018).

Table 3. Concentrations (mean ± standard deviation; min-max) of total PM$_{10}$ (expressed in µg/m^3) as well as As, Cd, Ni and Pb (expressed in ng/m^3) in 2013 and in May – July quarters of 2014-2018 for TO-Consolata (urban), Druento (rural) e TRM (sub-urban) sites.

Element	**2013**			**2014-2018 (May-July)**		
	TO-Consolata	Druento	TRM	TO-Consolata	Druento	TRM
PM$_{10}$	40 ± 28	24 ± 16	33 ± 23	21 ± 7	18 ± 3	18 ± 7
	(5 – 144)	(5 – 101)	(4 – 110)	(5 – 46)	(5 – 71)	(4 – 45)
As	0.71 ± 0.03	0.71 ± 0.03	0.71 ± 0.03	0.7	0.7	0.7
	(0.7 – 0.8)	(0.7 – 0.8)	(0.7 – 0.8)	(0.7 – 0.7)	(0.7 – 0.7)	(0.7 – 0.7)
Cd	0.23 ± 0.34	0.12 ± 0.04	0.22 ± 0.16	0.1	0.1	0.1
	(0.1 – 1.2)	(0.1 – 0.2)	(0.1 – 0.6)	(0.1 – 0.1)	(0.1 – 0.1)	(0.1 – 0.1)
Ni	4.88 ± 2.50	1.59 ± 1.14	2.95 ± 1.63	2.7 ± 1.3	3.0 ± 5.4	2.3 ± 1.2
	(2 – 11)	(0.7 – 3.8)	(0.7 – 5.8)	(0.7 – 5.4)	(0.7 – 23)	(0.7 – 5.3)
Pb	10 ± 6	4.2 ± 2.5	8.9 ± 5.6	4.2 ± 0.8	2.1 ± 0.8	3.1 ± 1.3
	(4 – 26)	(1 – 9)	(2 – 21)	(3 – 6)	(1 – 4)	(1 – 6)

No significant differences can be evidenced by Kruskal-Wallis test (significance level: 95%) due to the high variability of As, Cd, Ni and Pb concentrations in PM$_{10}$ samples, but it is however possible to make some general considerations. More precisely, relative to the whole year 2013, arsenic concentrations are similar in the three sites, while PM, cadmium and lead concentrations are higher in TO-Consolata site where the traffic and combustion phenomena are prevalent. Ni concentrations in the urban site are approximately thrice and twice higher that in the rural and sub-urban sites respectively. Considering, instead, the May-July quarters in the 2014-2018 period, it is evident that Cd and As concentrations are similar in the three sites, while Ni and Pb concentrations are lower in TRM site than in TO-Consolata site. Finally, relative to Druento, the Pb concentrations are higher and Ni concentrations are lower in TRM site. The anomalous Ni behavior can be explained taking into account that the Druento site is located in a large regional park and, therefore, in spring-summer it is more subject to episodes of soil dust resuspension that increase Ni concentrations in PM, due to the high background levels of this element in Piedmont soils (Biasioli et al., 2006; Bonifacio et al., 2010; Padoan et al., 2016); this is also confirmed by high variability of Ni concentrations in this site. The Pb behavior, instead, is a further confirmation of its possible anthropogenic input to the PM in TRM site. However, since Pb is one of the principal markers of incinerator emission, a further study of lead isotopic ratios was performed in order to identify the possible sources of lead in the airborne particulate matter collected in TRM site.

In addition, we compared our results with target metals found in PM_{10} emitted from Municipal Solid Waste Incinerators (MSWI) located in UK (Font et al., 2015), where As, Cd, Cr, Cu, Pb, Mn, Ni and V were considered as target pollutants of MSWI emissions. In all cases, considering maximum values, the element concentrations near such plants are several orders of magnitude higher than in TRM site (e.g., Pb concentration is 7.35 ng/m^3 in this study and 200 µg/m^3 in MSWI sites in UK (Font et al., 2015). This demonstrates that incinerators of new installation have a lower impact on atmospheric particulate matter composition thanks to current legislation and up-to-date technologies.

Moreover, to evaluate if the incinerator installed near Turin city influenced the PM_{10} composition, Cu/Pb, Cd/Cu, Cr/Pb, and Cd/Pb ratios were calculated and compared with the values reported for MSWI, rural and traffic emissions in Font et al. (2015). These ratios were used to discriminate between the different sources of potentially toxic metals in airborne particulate matter. Table 4 shows that average values of Cu/Pb, Cd/Cu and Cd/Pb calculated in this study are prevalently typical of traffic pollution. Therefore, we can assume that the major contribution in Cu, Pb and Cd to PM_{10} collected in TRM site is due to the traffic instead of being originated from the emissions of the incinerator. The high value found for Cr/Pb ratio is probably due to a relevant natural contribution for chromium from soils: as reported above, Piedmont plains originated during past fluvio-glacial events and are therefore made of sediments, which partly derive from serpentinitic areas; this, as already documented by other researchers (Biasioli et al., 2006; Bonifacio et al., 2010; Padoan et al., 2016), causes high background levels of Ni and Cr in soils and in soil dust.

Table 4. Typical Cu/Pb, Cd/Cu, Cr/Pb and Cd/Pb ratios calculated in this study compared with rural situation, MWI and traffic pollution (Font et al., 2015).

Ratio	This study	MSWI	Rural	Traffic
Cu/Pb	4.62	0.83	0.51	2.38
Cd/Cu	0.005	0.14	0.026	0.007
Cr/Pb	0.81	0.56	0.13	0.28
Cd/Pb	0.023	0.08	0.013	0.017

Finally, Enrichment Factors (EFs) were calculated with respect to the mean values for the Earth's upper crust reported by Wedepohl (1995), in order to distinguish elements having geologic or non-geologic origin. The equation used is the following:

$$EF_i = \frac{C_{i\ PM}/C_{r\ PM}}{C_{i\ crust}/C_{r\ crust}}$$

where $C_{i\ PM}/C_{r\ PM}$ and $C_{i\ crust}/C_{r\ crust}$ are the ratios between the concentration of the element *i* and the concentration of a reference element *r* respectively in the sample and in the upper crust; in this work, Al was selected as a reference element. By convention, EFs lower than 10 are taken as an indication that an element has a prevailing geogenic origin, EFs between 10 and 100 indicate a moderate enrichment and EFs higher than 100 indicate that the element (called "enriched") has a prevailing non-geogenic origin (Lai et al., 2017; Tahri et al., 2017).

The average values of EFs were reported in Figure 5.

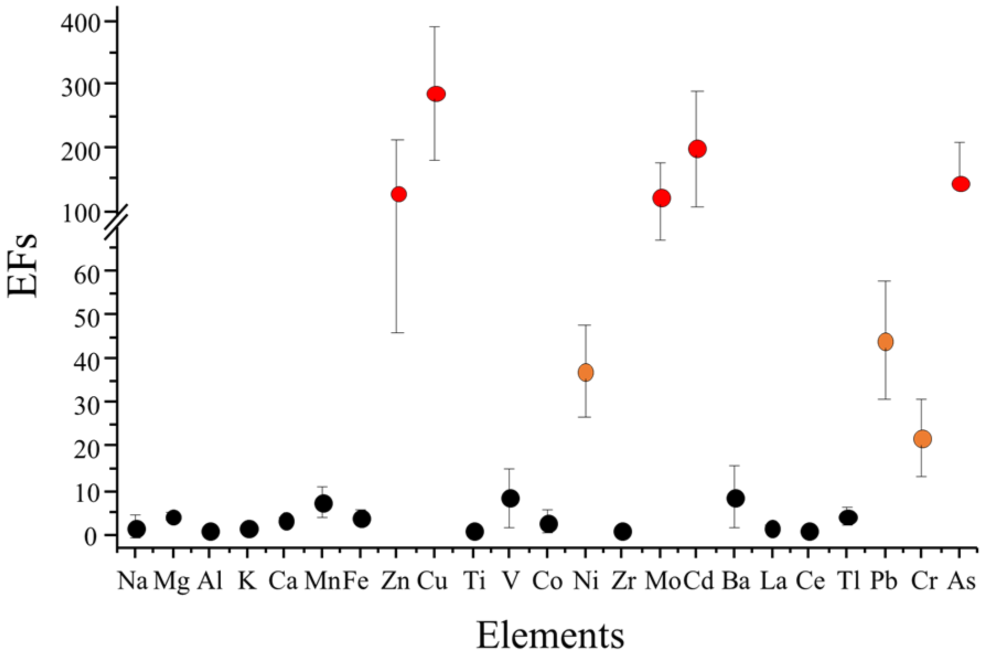

Figure 5. *Enrichment Factors for elements determined in* PM_{10} *samples.*

As, Cd, Cr, Cu, Mo, Ni, Pb and Zn are predominantly generated by anthropic activities, with EFs values higher than 10. These EFs are not higher than those reported for the city of Turin in previous studies (Padoan et al., 2016), which represents a further confirmation that the installation of MSWI plant did not lead to an increase in polluting emissions into the atmosphere. Finally, the elements moderately or highly enriched in this sampling station can arise from vehicle emissions which likely increased in this area due to the opening of the MSWI plant.

3.1.2 Water-soluble ions concentrations

The concentrations of major WSI and their contribution to the PM_{10} concentrations are shown in Table 5, where it can be seen that the respective average concentrations of the total WSI were 2.93, 8.87 and 5.16 μg/m^3 for May, June and July and accounted for 33.06%, 28.89% and 22.67% of the PM_{10} mass. The average percentage was equal to 28.21%, a percentage slightly lower compared to other studies (Ochsenkühn et al., 2008; Li et al., 2015) where WSI is equivalent to 40%, but higher compared to a different work (Fan et al., 2014), where WSI of 12% was measured. The concentrations of the WSI were dominated by NO_3^-, SO_4^{2-} and NH_4^+, followed by Ca^{2+}, Na^+, K^+, Mg^{2+} and Cl^-. It is also shown that secondary inorganic ions (SII: NO_3^-, SO_4^{2-} and NH_4^+) accounted for 77.37%, 89.13% and 87.98%, respectively, of the WSI for May, June and July. In Table 5, it can be seen that the mean concentrations of the total WSI were higher in June and July than in May: this is likely due to more consistent weather conditions in the two summer months.

Table 5. Mean and standard deviation (Mean ± SD), and 5th - 95th percentiles of major water-soluble ions (WSI), divided by month. All the concentrations are expressed in ng/m^3 except NH_4^+, NO_3^- and SO_4^{2-} which are expressed in μg/m^3.

	May		**June**		**July**	
Element	**Mean ± SD**	**5th - 95th perc.**	**Mean ± SD**	**5th - 95th perc.**	**Mean ± SD**	**5th - 95th perc.**
Cl^-	68 ± 110	19 – 234	20 ± 1	< 19 - 21	19 ± 1	< 19 – 21
NO_3^-	1.07 ± 0.9	0.48 – 2.48	4.8 ± 0.8	3.63 – 5.43	2.7 ± 0.5	2.23 – 3.53
SO_4^{2-}	0.90 ± 0.83	0.27 – 2.11	1.5 ± 0.5	0.81 – 2.03	0.83 ± 0.30	0.45 – 1.24
NH_4^+	0.30 ± 0.23	0.14 – 0.66	1.6 ± 0.2	1.34 – 1.94	0.99 ± 0.20	0.79 – 1.28
Ca^{2+}	203 ± 88	105 – 318	628 ± 196	351 – 830	411 ± 164	222 – 629
K^+	77 ± 22	46 – 103	134 ± 37	99 – 188	97 ± 19	78 – 123
Mg^{2+}	41 ± 43	10 – 107	57 ± 13	37 – 66	39 ± 12	23 – 54
Na^+	273 ± 383	29 – 873	125 ± 19	103 – 150	55 ± 16	33 – 73
SII	2266 ± 1916	922 – 5251	7909 ± 853	6816 – 9035	4538 ± 822	3729 – 5844
WSI	2928 ± 2475	1168 – 6654	8873 ± 825	7859 – 9981	5158 ± 883	4295 – 6525

More in detail, anions content is larger compared to the cations one (19.70% vs 8.51%), prevalently attributable to nitrates (13.08%) and sulfates (5.92%) produced by combustion processes in vehicles and industries respectively. The main component of WSI is overall ammonium nitrate (Pearson's correlation index between NH_4^+ and NO_3^- is 0.985).

It has been reported that the mass ratio of nitrate/sulphate can be used to evaluate the relative contribution of mobile and stationary sources in the atmosphere (Xu et al., 2012; Zhou et al., 2016). The mass ratios of

NO_3^-/SO_4^{2-} in May, June and July were 1.19, 3.18 and 3.26 respectively; they were therefore greater than one, and this was especially true in June and July, which indicates that mobile sources (e.g. vehicle exhaust) make a greater contribution to aerosol pollution than stationary sources (e.g. incinerator). It should be noted that the mass ratios of NO_3^-/SO_4^{2-} increased greatly in the two summer months, which suggests that the vehicular traffic may have a more important effect on the PM_{10} concentration in the investigated area when the weather conditions are more stable.

Finally, higher concentrations of Na^+ and Cl^- were found in May (Figure 6), when also the second combustion line of the incinerator was active. Direct incinerator emissions are conceivable sources for these ions: Na is used such as $NaHCO_3$ at the Turin incinerator plant for the abatement of acids from vapor emissions (http://trm.to.it/) and, hence, it can combine with hydrochloric acid present in gaseous fumes arising from the combustion of organic chlorine present in waste (e.g. plastics, PVC, chlorinated solvents); NaCl can also be already present in the form of salt contained in paper and cardboard, food and vegetable waste. Moreover, it is interesting to note that, in May, when the NaCl concentration is higher, the NH_4NO_3 concentration is lower. This represents a further confirmation that NaCl is one of the main sinks of NH_4NO_3 in the aerosol (Ochsenkühn et al., 2008).

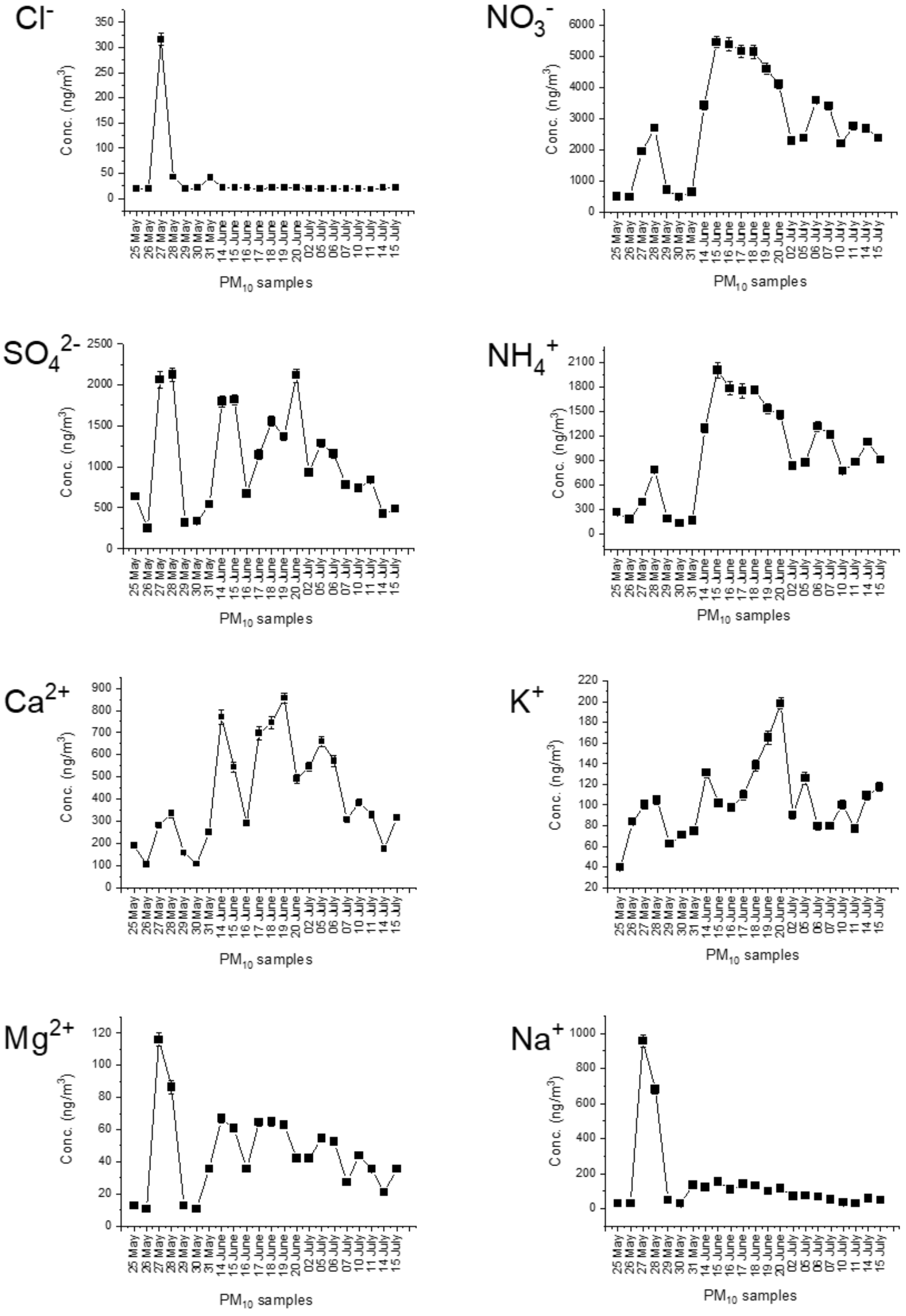

Figure 6: Concentration trends during start-up phase of the incinerator for water-soluble ionic components.

3.2 Optimization of instrumental parameters for Pb isotope ratios analysis

The optimization of the experimental conditions of the instrumental parameters for Pb isotope ratios was carried out following the factorial design of experiments and response surface methodology, originally developed by Box and Wilson. In order to reduce the number of measurements we decide to perform a Central Composite Design (CCD) considering four instrumental parameters at the same time. In Table 6 are reported the experimental parameters and the investigated ranges. A total of 24 different operative conditions plus 3 central points were considered.

Table 6. Investigated instrumental parameters and their range.

INSTRUMENTAL PARAMETERS	*LOW*	*INTERMEDIATE*	*HIGH*
Integration window (%)	60	80	100
Sampling points per peak	5	17	30
Run	1	5	9
Passes	1	5	9

Experiments were carried out randomly, both in low and medium resolution, using the two concentrations of SRM 981 standard (2.5 and 25 µg/L). Blank signal was subtracted for all the tests, and the interference of ^{204}Hg was considered with respect to ^{204}Pb by calculating mathematically the amount of this isotope after measuring ^{202}Hg that is not affected by any spectral interferences.

For each experiment the total accuracy was evaluated, that is the average of the absolute value of the accuracies for every isotope, together with the precision, that is the relative standard deviation of the accuracy for all the isotopes. Both accuracy and precision are expressed as percentages. Table 7 reports the results obtained for all the meaningful experiments in low and medium resolution, with the accuracy and the precision at SF-ICP-MS, at both 2.5 µg/L and 25 µg/L concentration of NIST SRM 981.

Table 7. Experiments set selected by CCD and carried out in LR (low resolution) and MR (medium resolution) for the 2.5 and 25 µg/L of SRM981 concentration (results for experiments N2, N10, N13, N14 and N18 are not reported because of the too low number of sampling points per peak).

Experiment	Accuracy 2.5 µg/L LR	Precision 2.5 µg/L LR	Accuracy 25 µg/L LR	Precision 25 µg/L LR	Accuracy 2.5 µg/L MR	Precision 2.5 µg/L MR	Accuracy 25 µg/L MR	Precision 25 µg/L MR
N1	2.59	2.05	5.45	6.8	17.35	8.34	11.29	13.05
N3	4.19	2.04	6.53	1.01	7.24	5.21	9.46	1.47
N4	4.77	5.64	2.73	1.77	7.06	6.01	1.2	0.41
N5	2.02	1.91	4.31	1.45	5.89	2.19	2.78	1.92
N6	9.84	11.02	2.28	3.11	8.6	8.93	4.55	0.17
N7	1.53	1.56	1.6	1.75	3.19	3.43	0.74	0.78
N8	1.05	1.2	1.62	1.62	1.66	0.86	3.94	1.33
N9	2.74	0.65	2.93	2.45	2.33	2.96	5.03	5.92
N11	0.83	0.97	1.95	2.01	2.73	3.17	1.32	0.52
N12	1.01	1.33	0.57	0.09	3.56	4.34	3.06	2.89
N15	1.06	1.06	1.05	1.06	0.82	0.98	0.96	0.75
N16	1.52	1.31	1.01	1.1	2.41	1.75	0.92	1.12
N17	1.24	1.14	1.24	1.54	0.94	0.75	0.95	0.73
N18	2.19	2.14	2.6	1.29	3.1	1.36	0.62	0.67
N20	1.46	1.44	0.74	0.84	4.91	2.76	5.77	2.53
N21	4.21	3.34	2.12	1.44	5.7	5.08	4.15	3.71
N22	0.8	0.94	1.97	1.02	3.77	1.7	0.87	0.77
N23	2.65	2.75	2.43	2	4.19	3.71	3.89	2.02
N24	1.63	1.75	1.26	1.49	1.21	1.46	1.05	0.83
N25	2.34	2.43	1.85	0.79	1.05	0.78	1.19	0.84
N26	3.64	1.33	2.77	2.16	1.35	1.7	2.96	0.72
N27	2.64	1.97	0.61	0.58	0.8	0.89	2.43	2.22

Four groups of tests (responses) were carried out, for the two concentrations of NIST SRM 981 (2.5 and 25 µg/L) in low and medium resolution. A PLS (Partial Least Square) regression was applied to obtain a second-order model by projecting the predicted variables and the observable ones to a new space considering accuracy, precision and the four variables aforementioned. Variables were scaled at unit variance when the model was fitted. The results were used to provide the minimum values of accuracy and precision (expressed in percentages) depicted in green in Figure 7.

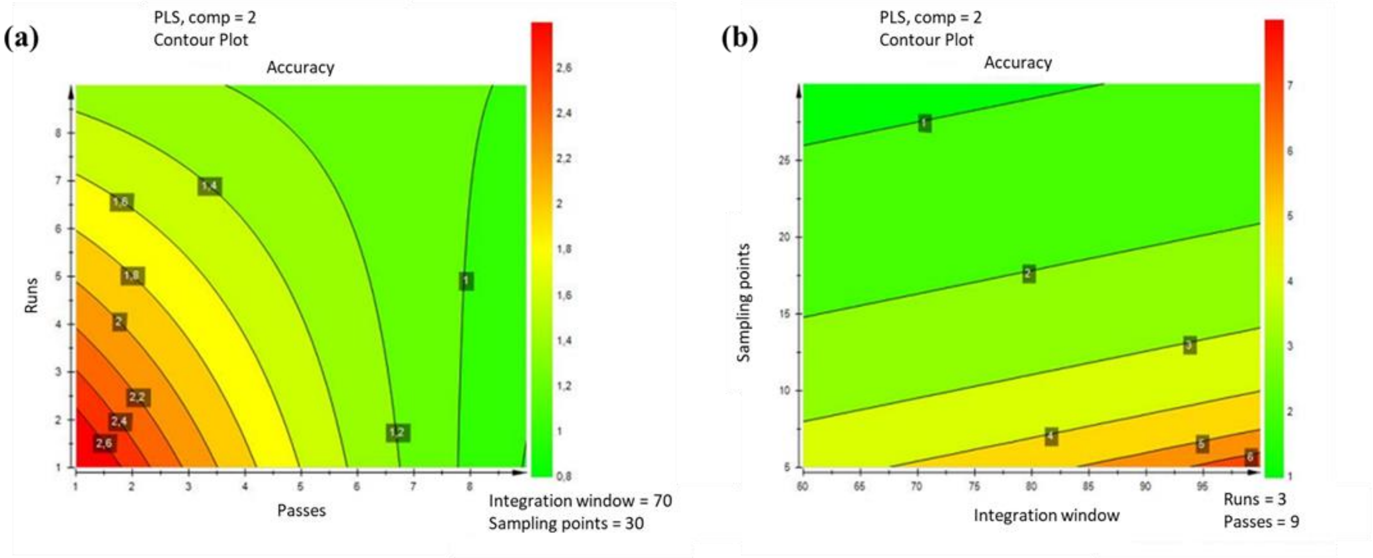

Figure 7: *The effect of runs and passes (a) and sampling points and integration window (b) on accuracy of lead isotope ratios determination.*

In this way we were able to identify the experimental conditions with the closer values to the certified one and with minimum dispersion.

Among the four variables, sample points per peak was the most important one respect to accuracy and precision. The optimum response was obtained using 2.5 µg/L of SRM 981 concentration in low resolution. The related optimal values of the four variables (3 runs, 9 passes, 70% of integration window and 30 sampling points per peak) produced values equal to a 0.83 ± 0.46% of accuracy and 0.75 ± 0.42% of precision. Those operative conditions were successfully used in the isotopic investigation of lead for the PM_{10} samples.

3.3 Lead isotope ratios determination

Lead concentration is low in all the samples analyzed, with values between 0.8 ng/m^3 (during May) and 7.4 ng/m^3 (during June). EFs are in the range between 26.4 and 71.9, indicating a slightly anthropogenic contribution for Pb in the PM_{10} samples.

Lead isotope ratios for all PM_{10} samples (Tables 8 and 8S) were determined, by adopting the optimized experimental conditions previously described (paragraph 3.3), in order to identify more accurately the possible sources of this element in the investigated area.

Table 8. Mean and standard deviation (Mean ± SD), median, and 5th - 95th percentiles of the lead isotope ratios (namely $^{204}Pb/^{206}Pb$, $^{206}Pb/^{207}Pb$ and $^{208}Pb/^{206}Pb$ ratios) according to the month.

$^{204}Pb/^{206}Pb$	**May**	**June**	**July**
Mean ± SD	0.0532 ± 0.0008	0.0545 ± 0.0021	0.0514 ± 0.0013
Median	0.0532	0.0551	0.0508
5th - 95th perc.	0.0519 – 0.0540	0.0515 – 0.0566	0.0502 – 0.0533
$^{206}Pb/^{207}Pb$	**May**	**June**	**July**
Mean ± SD	1.1595 ± 0.0066	1.1578 ± 0.0166	1.1766 ± 0.0325
Median	1.1601	1.1643	1.1908
5th - 95th perc.	1.1502 – 1.1670	1.1327 – 1.1711	1.1351 – 1.2102
$^{208}Pb/^{206}Pb$	**May**	**June**	**July**
Mean ± SD	2.0347 ± 0.124	1.9952 ± 0.0581	1.9300 ± 0.0550
Median	2.0922	2.0176	1.9106
5th - 95th perc.	1.8507 – 2.1216	1.9059 – 2.0473	1.8806 – 2.0143

With a view to monitor accuracy together with precision of measurements, periodical readings of SRM 981 were performed.

With the aim to define which are the sources of lead in the PM_{10} samples, the isotopic signature of each possible source for Pb should be known. This signature is a consequence of the mineral characteristic of the soil or of the material from which industrial lead was extracted. Generally, it was observed that atmospheric Pb was mainly influenced by traffic during the first part of Nineties of the twentieth century, followed by a mixed influence on traffic and industry during the 1995-1999 period. After 2000, when leaded gasoline was forbidden in Europe, the greatest part of atmospheric lead is coming from industrial activities (De la Cruz et al., 2009; Widory et al., 2004).

While each lead source has its own specific isotopic composition, it is useful to note that separate geochemical reservoirs are linked together and the final isotopic composition of lead results from mixing of many diverse sources.

Tropospheric lead, when is produced by anthropic activities, is mostly associated with the submicrometric aerosols that can be transported over long distances making thus the interpretation of lead isotopic data not easy (Flament et al., 2002).

In addition, the isotopic composition of lead changes quickly depending on the different inputs for this element, distance from industrial areas, traffic density, prevailing wind directions and rainfall intensity (Simonetti et al., 2000).

In Europe, an important increase of the $^{206}Pb/^{207}Pb$ ratio (from 1.09 to 1.17) was observed from the end of the 19th to the end of 20th century. This increase can be explained by several causes, such as a significant import of ores with less radiogenic ratios, modifications in industrial practices, combustion process of coal originating from different areas of the world (Bacon et al., 1996).

A further increase of the $^{206}Pb/^{207}Pb$ ratio was caused by the introduction of leaded gasoline throughout the world. The subsequent decrease of the $^{206}Pb/^{207}Pb$ ratio (to 1.09) in the 1980s reflects the gradual abandoning of leaded gasoline throughout Europe. These changes are associated with a decisive contraction of atmospheric lead concentrations.

Values obtained in this work for the lead isotopes, in terms of $^{208}Pb/^{206}Pb$ and $^{206}Pb/^{207}Pb$ ratios, are comparable to those found in the literature for countries from the Northern Hemisphere (De la Cruz et al., 2009; Bollhöfer and Rosman, 2001) even if a higher radiogenic contribute was found respect to previous works performed in Venice between 1998 and 1999. Firstly, in that case the concentration of lead was higher (13-22 ng/m^3) due to the presence of lead in gasoline in that period. Moreover, the values found for ^{208}Pb/^{207}Pb ratio (2.42-2.43) are comparable, denoting a variation only in the contribution of the radiogenic isotope (^{206}Pb) (Bollhöfer and Rosman, 2001).

Lead isotopic ratios determined in the PM$_{10}$ samples collected in TRM site are reported as ^{208}Pb/^{206}Pb vs ^{206}Pb/$^{/207}$Pb ratios in figure 8.

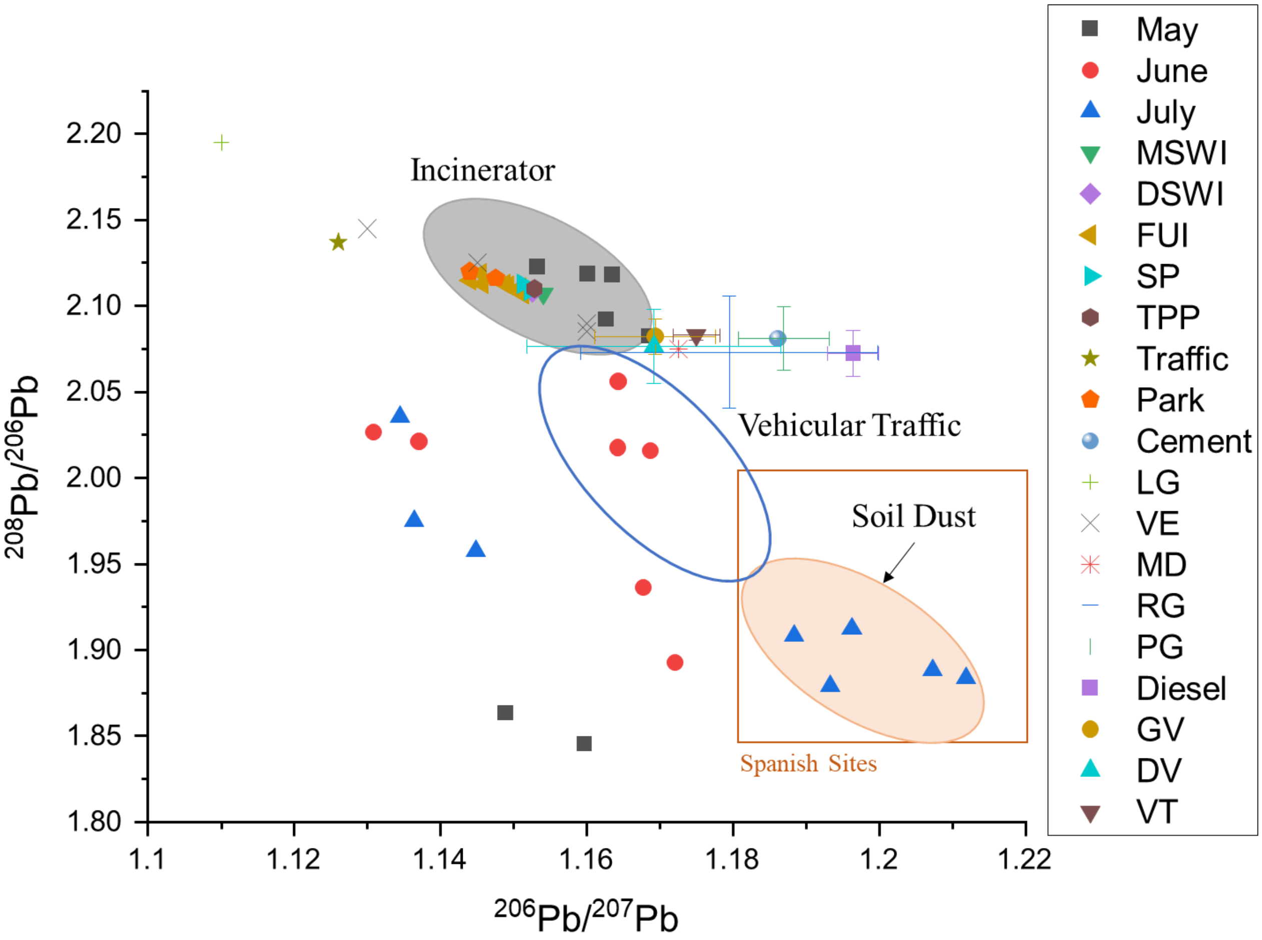

***Figure 8**: Plot of ^{208}Pb/^{206}Pb vs ^{206}Pb/^{207}Pb ratios for PM$_{10}$ samples collected in TRM site and in several source samples from literature data: MSWI (Carignan et al., 2005); DSWI – Domestic Solid Waste Incinerator, FUI – French Urban Incinerator, SP – Steel Plant, TPP – Thermal Power Plant, Traffic, Park,*

Cement (Lahd Geagea et al., 2008); LG – Loaded Gasoline, VE – Vehicle Exhaust, MD – Metallurgic Dust (Xu et al., 2020); RG – Regular Gasoline, PG – Premium Gasoline, Diesel, GV – Gasoline Vehicular, DV – Diesel Vehicular, VT – Vehicular Traffic (Gioia et al., 2017); Spanish Sites (Kylander et al., 2010).

A partial separation of July samples from May and June samples can be observed; most of the July samples, indeed, present low values for both ^{206}Pb/$^{/207}$Pb and ^{208}Pb/^{206}Pb ratios. A distinction between May and June samples is not evident, even if May samples show intermediate values for the ^{206}Pb/$^{/207}$Pb ratios and a greater variability in the values for ^{208}Pb/^{206}Pb ratios, whereas the June samples are characterized by higher values for the ^{206}Pb/$^{/207}$Pb ratios and intermediate values for ^{208}Pb/^{206}Pb ratios.

Thus, comparing these results with other studies (Widory et al., 2004; Komárek et al., 2006; Novák et al., 2003; Teutsch et al., 2001; Carignan et al, 2005; Lahd Geagea et al., 2008; Guéguen et al., 2012; Gioia et al., 2010, 2017; Zhao et al., 2019; Lee et al., 2019; Xu et al. 2020), it is possible to speculate a principally geogenic contribution for lead in PM$_{10}$ samples collected in July since the lead isotope ratios found in most of these samples are more characteristic of European ores. Indeed, the ^{206}Pb/$^{/207}$Pb ratios ranged from 1.8833 to 1.2119, with an average value of 1.1994, similar to the results reported by Kylander et al. (2010), Kelepertzis et al. (2016) and Zhao et al. (2019), in which the natural end member of parent material showed higher ^{206}Pb/$^{/207}$Pb ratios compared with the anthropogenic-related sources. For example, the major soil dust emitting areas on a global scale, including the Sahara–Sahel area (Abouchami and Zabel, 2003), Gobi desert (Biscaye, et al., 1997) and European loess soils (Klaminder, et al., 2003; Sterckeman et al., 2006), have ^{206}Pb/^{207}Pb ratios varying between 1.19 and 1.25. The PM$_{10}$ samples collected in June, instead, seem be more influenced by vehicular traffic (^{206}Pb/$^{/207}$Pb ratios ranged from 1.1308 to 1.1721, with the average value of 1.1578). Indeed, these data fit well with ^{206}Pb/$^{/207}$Pb ratios determined by Gioia et al. (2010 and 2017) for several traffic sources and suggest that the main source of lead in these samples is represented by vehicular traffic. Finally, it is particularly noteworthy that most of the PM$_{10}$ samples collected in May display ^{208}Pb/^{206}Pb and ^{206}Pb/$^{/207}$Pb ratios similar to values reported for several European MSWI plants

(Carignan et al, 2005; Geagea et al., 2008; Guéguen et al., 2012). The chemical and isotopic characterization of Pb emitted by MSWI plants is not an easy task because of the extreme heterogeneity of waste materials processed in these plants. Moreover, MSWI plants represent themselves a significant source of metals to the atmosphere. Nevertheless, the Pb isotopic composition for this source, reported in the literature (Carignan et al., 2005; Lahd Geagea et al., 2008 Guéguen et al., 2012), is fairly homogeneous and is defined by a restricted range in $^{206}Pb/^{207}Pb$ and $^{208}Pb/^{206}Pb$ values, 1.148-1.158 and 2.101-2.114 respectively, compared to other environmental samples. In conclusion, it is evident that the higher Pb content is not indicative of a greater contribution of this element to PM_{10} due to the MSWI commissioning because, during start-up phase, the lowest concentration for this element was observed in May (range: 0.54-2.27, mean: 1.17 ng/m^3) and it increased in June and July (range: 2.73-7.35, mean: 1.58 in June and range: 2.26-4.36, mean: 3.16 in July). The commissioning of second line of combustion from 22 May to 5 June could be the most likely explanation for the greater influence of incinerator emissions on PM_{10}, evidenced by the Pb isotope ratios at the end of May. In July, when the MSWI plant has likely entered full capacity, it is possible that the Pb isotope ratios represent the typical sources influencing the PM_{10} in the investigated area, i.e. vehicular traffic and soil dust.

Conclusions

In conclusion, vehicular traffic was identified as the main atmospheric pollution source for PM_{10} samples collected near Turin MSWI plant. EFs and element concentrations are comparable with those reported for other sites located in the city of Turin confirming that the installation of MSWI plant did not lead to an overall increase in polluting emissions into the atmosphere. The elements moderately or highly enriched (Cr, Ni, Cu, Zn, As, Mo, Cd and Pb) seem to arise mainly from vehicle emissions which likely increased in this area after the opening of the MSWI plant due to heavier traffic of trucks carrying the wastes. This source of tropospheric pollution affects also lead concentration, as confirmed by lead isotope ratios determined by a method that was developed and optimized using an experimental design approach.. However, a possible crustal contribution in July and a possible influence of the incinerator in May have been highlighted taking into account the lead isotope ratios determined in PM_{10} samples collected in these two months.

Further studies about lead isotope ratios and PM_{10} elemental composition should be done in the same area of sampling during incinerator activity for defining a possible long-term impact of the plant in the Turin suburban area.

References

Abouchami W., Zabel M., 2003. Climate forcing of the Pb isotope record of terrigenous input into the Equatorial Atlantic. Earth Planet. Sci. Lett. 213, 221–234. DOI: 10.1016/S0012-821X(03)00304-2.

Amato, F. Non-exhaust emissions; Elsevier: 2018.

Arpa Piemonte, Rapporto di sintesi sui dati prodotti dalla stazione di monitoraggio della qualità dell'aria ubicata nel Comune di Beinasco – Giardino Pubblico Aldo Mei, di proprietà di TRM S.p.A. Anno 2013.

Arpa Piemonte, 2013. Uno sguarda all'aria.

Arpa Piemonte, 2014. Uno sguarda all'aria.

Arpa Piemonte, 2015. Uno sguarda all'aria.

Arpa Piemonte, 2016. Uno sguarda all'aria.

Arpa Piemonte, 2017. Uno sguarda all'aria.

Arpa Piemonte, 2018. Uno sguarda all'aria.

Bacon J.R., Jones K.C., McGrath S.P., Johnston A.E., 1996. Isotopic character of lead deposited from the atmosphere at a grassland site in the United Kingdom since 1860. Environ. Sci. Technol. 30, 2511–2518. DOI: 10.1021/es950839s.

Biasioli M., Barberis R., Ajmone-Marsan F., 2006. The influence of a large city on some soil properties and metals content. Sci. Total Environ. 356, 154-164. DOI: 10.1016/j.scitotenv.2005.04.033.

Birmili W., Allen A.G., Bary F., Harrison R.M., 2006. Trace metal concentrations and water solubility in size-fractionated atmospheric particles and influence of road traffic. Environ.Sci.Technol. 40, 1144-1153. DOI: 10.1021/es0486925.

Biscaye P.E., Grousset F.E., Revel M., Gaast V.S., Zielinski G.A., Vaars A., Kukla G., 1997. Asian provenance of glacial dust (stage 2) in the Greenland Ice Sheet Project 2 ice core Summit Greenland. J. Geophys. Res. 102, 26765–26781. DOI: 10.1029/97JC01249.

Bollhöfer A., Rosman K.J.R., 2000. Isotopic source signatures for atmospheric lead: The Southern Hemisphere. Geochim. Cosmochim. Acta 64, 3251–3262. DOI: 10.1016/S0016-7037(00)00436-1.

Bollhöfer A., Rosman K.J.R., 2001. Isotopic source signatures for atmospheric lead: The Northern Hemisphere. Geochim. Cosmochim. Acta. 65, 1727-1740. DOI: 10.1016/S0016-7037(00)00630-X.

Bonifacio E., Falsone G., Piazza S., 2010. Linking Ni and Cr concentrations to soil mineralogy: does it help to assess metal contamination when the natural background is high? J. Soils Sediments 10, 1475-1486. DOI: 10.1007/s11368-010-0244-0.

Carignan J., Libourel G., Cloquet C., Le Forestier L., 2005. Lead isotopic composition of fly ash and flue gas residues from municipal solid waste combustors in France: implications for atmospheric lead source tracing. Environ. Sci. Technol. 39, 2018-2024. DOI: 10.1021/es048693x.

Cohen J., Cohen P., West S.G., Aiken L.S., 2003. Applied multiple regression/correlation analysis for the behavioral sciences. 3rd ed. Lawrence Erlbaum Associates, Inc., Mahwah, New Jersey.

Conca E., Malandrino M., Giacomino A., Inaudi P., Buoso S., Bande S., Sacco M., Abollino O., 2020. Contribution of the incinerator to the inorganic composition of the PM_{10} collected in Turin, Atmosphere-Basel, 11, 400. DOI: 10.3390/atmos11040400.

Councell T.B., Duckenfield K.U., Landa E.R., Callender E., 2004. Tire-wear particles as a source of zinc to the environment. Environ. Sci. Technol., 38, 4206-4214. DOI: 10.1021/es034631f.

Decreto Ministeriale n 60 02/04/2002 from Council Directive 1999/30/EC of 22 April 1999.

De la Cruz M.T., Laborda F., Callén M.S., López J.M., Mastral A.M., 2009. Study of Pb sources by Pb isotope ratios in the airborne PM10 of Zaragoza, Spain. J. Environ. Monit. 11, 2052-2057. DOI: 10.1039/b912274e.

Directive 2000/76/EC of the European Parliament and of the Council of 28 December 2010 on the incineration of waste (the WI Directive).

Directive 2008/50/EC of the European Parliament and of the Council of 21 May 2008 on ambient air quality and cleaner air for Europe.

D.Lgs. 155, 2010. Official Gazette of the Italian Republic, 216.

European Environment Agency (EEA), 2013. Air quality in Europe – 2013 report 9/2013.

European Environment Agency (EEA), 2015. Air quality in Europe – 2015 report 5/2015.

Fan J., Yue X.Y., Jing Y., Chen Q., Wang S.G., 2014. Online monitoring of water-soluble ionic composition of PM10 during early summer over Lanzhou City. J. Environ. Sci. 26, 353–361. DOI: 10.1016/S1001-0742(13)60431-3.

Flament P., Bertho M.L., Deboudt K., Veron A., Puskaric E., 2002. European isotopic signatures for lead in atmospheric aerosols: a source apportionment based upon Pb-206/Pb-207 ratios. Sci. Total. Environ. 296, 35–57. DOI: 10.1016/S0048-9697(02)00021-9.

Font A., de Hoogh K., Leal-Sanchez M., Ashworth D.C., Brown R.J.C., Hansell A.L., Fuller G.W., 2015. Using metal ratios to detect emissions from municipal waste incinerators in ambient air pollution data. Atmos. Environ. 113, 177-186. DOI: 10.1016/j.atmosenv.2015.05.002.

Gao J.J., Tian H.Z., Cheng K., Lu L., Zheng M., Wang S.X., Hao J.M., Wang K., Hua S.B., Zhu C.Y., Wang Y., 2015. The variation of chemical characteristics of PM2.5 and PM10 and formation causes during two haze pollution events in urban Beijing, China. Atmos. Environ. 107, 1-8. DOI: 10.1016/j.atmosenv.2015.02.022.

Gerhardsson L., 2004. Lead In: Merian E., Anke M., Ihnat M., Stoeppler M. (Eds.), Elements and their compounds in the environment, WILEY-VCH Verlag GmbH&Co. KGaA, Weinheim, 879-900.

Gholampour A., Nabizadeh R., Hassanvand M.S., Taghipour H., Rafee M., Alizadeh Z., Faridi S., Mahvi A.H., 2016. Characterization and source identification of trace elements in airborne particulates at urban and suburban atmospheres of Tabriz, Iran. Environ. Sci. Pollut. Res. Int. 23, 1703-1713. DOI: 10.1007/s11356-015-5413-7.

Gioia, S.M.C.L., Babinski, M., Weiss, D.J., Kerr, A.A.F.S., 2010. Insights into the dynamics and sources of atmospheric lead and particulate matter in São Paulo, Brazil, from high temporal resolution sampling. Atmos. Res. 98, 478-485. DOI: 10.1016/j.atmosres.2010.08.016.

Gioia S.M.C.L., Babinski M., Weiss D.J., Spiro B., Kerr A.A.F.S., Veríssimo T.G., Ruiz I., Prates J.C.M., 2017. An isotopic study of atmospheric lead in a megacity after phasing out of leaded gasoline Atmos. Environ. 149, 70-83. DOI: 10.1016/j.atmosenv.2016.10.049.

Guéguen F., Stille P., Lahd Geagea M., Perrone T., Chabaux F., 2012. Atmospheric pollution in an urban environment by tree bark biomonitoring – Part II: Sr, Nd and Pb isotopic tracing, Chemosphere 86, 641–647. DOI: 10.1016/j.chemosphere.2011.11.008.

Harrison R.M., Jones A.M., Gietl J., Yin J., Green D.C., 2012. Estimation of the contributions of brake dust, tire wear, and resuspension to non-exhaust traffic particles derived from atmospheric measurements. Environ. Sci. Technol. 46, 6523-6529. DOI: 10.1021/es300894r.

http://trm.to.it/ (Date of access: 12 November 2020).

https://umetrics.com/product/modde (Date of access: 20 October 2014).

International Agency for Research on Cancer (IARC), 2012. IARC monographs on evaluation of carcinogenic risk of chemicals to humans. A review of human carcinogens: arsenic, metals, fibres, and dusts, Vol. 100 C. Lyon, France: World Health Organization.

Kelepertzis E., Komárek M., Argyrakia A., Šillerová H., 2016. Metal(loid) distribution and Pb isotopic signatures in the urban environment of Athens, Greece. Environ. Pollut. 213, 420-431. DOI: 10.1016/j.envpol.2016.02.049.

Klaminder J., Renberg I., Bindler R., Emteryd O., 2003. Isotopic trends and background fluxes of atmospheric lead in northern Europe: analyses of three ombrotrophic bogs from south Sweden. Global Biogeochem. Cy. 17, 1019. DOI: 10.1029/2002GB001921.

Komárek M., Chrastný V., Ettler V., Tlustoš P., 2006. Evaluation of extraction/digestion techniques used to determine lead isotopic composition in forest soils. Anal. Bioanal. Chem. 385, 1109–1115. DOI: 10.1007/s00216-006-0543-x.

Komarek M., Ettler V., Chrastný V., Mihaljevic M., 2008. Lead isotopes in environmental sciences: a review. Environ. Int. 34, 562-577. DOI: 10.1016/j.envint.2007.10.005

Kylander M.E., Klaminder J., Bindler R., Weiss D.J., 2010. Natural lead isotope variations in the atmosphere. Earth Planet. Sc. Lett. 290, 44–53. DOI: 10.1016/j.epsl.2009.11.055.

Lahd Geagea M., Stille P., Gauthier - Lafaye F., Millet M., 2008. Tracing of industrial aerosol sources in an urban environment using Pb, Sr, and Nd isotopes. Environ. Sci. Technol. 42, 692–698. DOI: 10.1021/es071704c.

Lai A.M., Shafer M.M., Dibb J.E., Polashenski C.M., Schauer J.J., 2017. Elements and inorganic ions as source tracers in recent Greenland snow. Atmos. Environ. 164: 205-215. DOI: 10.1016/j.atmosenv.2017.05.048.

Lee S., Shin D., Han C., Choi K.S., Hur S.D., Lee J., Byun D.S., Kim Y.T., Hong S., 2019. Characteristic concentrations and isotopic composition of airborne lead at urban, rural and remote sites in western Korea. Environ. Pollut. 254, 113050. DOI: 10.1016/j.envpol.2019.113050.

Li T.C., Yuan C.S., Lo K.C., Hung C.H., Wu S.P, Tong C., 2015. Seasonal variation and chemical characteristics of atmospheric particles at three islands in the Taiwan strait. Aerosol Air Qual. Res. 15, 2277–2290. DOI: 10.4209/aaqr.2015.03.0153.

Lucarelli F., Barrera V., Becagli S., Chiari M., Giannoni M., Nava S., Traversi R., Calzolai G., 2019. Combined use of daily and hourly data sets for the source apportionment of particulate matter near a waste incinerator plant. Environ. Pollut. 247, 802-811. DOI: 10.1016/j.envpol.2018.11.107.

Lundstedt T., Seifert E., Abramo L., Thelin B., Nystrom A., Pettersen J., Bergman R., 1998. Experimental design and optimization. Chemom. Intell. Lab. Syst. 42, 3-40.

Malandrino M., Di Martino M., Ghiotti G., Geobaldo F., Grosa M.M., Giacomino A., Abollino O., 2013. Inter-annual and seasonal variability in PM10 samples monitored in the city of Turin (Italy) from 2002 to 2005. Microchem. J. 107, 76-85. DOI: 10.1016/j.microc.2012.05.026.

Meyer P.A., Brown M.J., Falk H. 2008. Global approach to reducing lead exposure and poisoning. Mutat. Res. Rev. Mutat. Res. 659, 166-175. DOI: 10.1016/j.mrrev.2008.03.003.Novák M., Emmanuel S., Vile M.A., Erel Y., Véron A., Pačes T., Wieder R.K., Vaněček M, Štěpánová M, Břízová E., Hovorka J., 2003.

Origin of lead in eight European peat bogs determined from isotope ratios, strengths, and operation times of regional pollution sources. Environ. Sci. Technol. 37, 437–445. DOI: 10.1021/es0200387.

Ochsenkühn K.M., Lyberopoulou T., Koumarianou G., Ochsenkühn-Petropoulou M., 2008. Ion chromatographic and spectrometric determination of water-soluble compounds in airborne particulates, and their correlations in an industrial area in Attica, Greece. Microchim. Acta. 160, 485–492. DOI: 10.1007/s00604-007-0830-z.

Pacyna E.G., Pacyna J.M., Fudala J., Strzelecka-Jastrzab E., Hlawiczka S., Panasiuk D., Nitter S., Pregger T., Pfeiffer H., Friedrich R., 2007. Current and future emissions of selected heavy metals to the atmosphere from anthropogenic sources in Europe. Atmos. Environ. 41, 8557e8566. DOI: 10.1016/j.atmosenv.2007.07.040.

Padoan E., Malandrino M., Giacomino A., Grosa M., Lollobrigida F., Martini S., Abollino O., 2016. Spatial distribution and potential sources of trace elements in PM10 monitored in urban and rural sites of Piedmont Region. Chemosphere 145, 495–507. DOI: 10.1016/j.chemosphere.2015.11.094.

Pakkanen T., Loukkola K., Kohonen C., Aurela M., Mäkelä T., Hillamo, R., Aarnio P., Koskentalo T., Kousa A., Maenhaut W., 2001.Sources and chemical composition of atmospheric fine and coarse particles in the Helsinki area. Atmos. Environ. 35, 5381-5391. DOI: 10.1016/S1352-2310(01)00307-7.

Panepinto D., Zanetti M.C., 2018. Municipal solid waste incineration plant: A multi-step approach to the evaluation of an energy-recovery configuration. Waste Manage. (Oxford) 73, 332-341, DOI: 10.1016/j.wasman.2017.07.036.

Poschl U., 2005. Atmospheric aerosols. Composition, transformation, climate and health effects. Angew. Chem. Int. Edit. 44, 7520-7540. DOI: 10.1002/anie.200501122.

Raffaelli K., Deserti M., Stortini M., Amorati R., Vasconi M., Giovannini G., 2020. Improving air quality in the Po Valley, Italy: some results by the LIFE-IP-PREPAIR Project. Atmosphere 11, 429. DOI:10.3390/atmos11040429.

Rokach L., Maimon O., 2005. Clustering methods. Data mining and knowledge discovery handbook. Springer, Boston, US.

Sakata M., Kurata M., Tanaka, N., 2000. Estimating contribution from municipal solid waste incineration to trace metal concentrations in Japanese urban atmosphere using lead as a marker element. Geochem. J. 34, 23-32. DOI: 10.2343/geochemj.34.23.

Simonetti A., Gariépy C., Carignan J., 2000. Pb and Sr isotopic compositions of snowpack from Québec, Canada: inferences on the sources and deposition budgets of atmospheric heavy metals. Geochim Cosmochim. Acta 64, 5–20. DOI: 10.1016/S0016-7037(99)00207-0.

Sterckeman T., Douay F., Baize D., Fourrier H., Proix N., Schvartz C., Carignan J., 2006. Trace element distributions in soils developed in loess deposits from northern France. Eur. J. Soil Sci. 57, 392–410. DOI: 10.1111/j.1365-2389.2005.00750.x.

Tahri M., Benchrif A., Bounakhla M., Benyaich F., Noack Y., 2017. Seasonal variation and risk assessment of PM2.5 and PM2.5-10 in the ambient air of Kenitra, Morocco. Environ. Sci.-Proc. Imp. 19: 1427-1436. DOI: 10.1039/c7em00286f.

Teutsch N., Erel Y., Halicz L., Banin A., 2001. Distribution of natural and anthropogenic lead in Mediterranean soils. Geochim. Cosmochim. Acta 65, 2853–2864. DOI: 10.1016/S0016-7037(01)00607-X.

Tong S., von Schirnding Y.E.; Prapamontol T., 2000. Environmental lead exposure: a public health problem of global dimensions. Bull. World Health Organ. 78, 1068-1077.

Vinceti M., Malagoli C., Teggi S., Fabbi S., Goldoni C., De Girolamo G., Ferrari P., Astolfi G., Rivieri F., Bergomi M., 2008. Adverse pregnancy outcomes in a population exposed to the emissions of a municipal waste incinerator. Sci. Total Environ. 407, 116–121. DOI: 10.1016/j.scitotenv.2008.08.027.

Wedepohl H., 1995. The composition of the continental crust. Geochim. Cosmochim. Acta 59, 1217-1232.

Widory D., Roy S., Le Moullec Y., Goupil G., Cocherie A., Guerrot C., 2004. The origin of atmospheric particles in Paris: a view through carbon and lead isotopes. Atmos. Environ. 38, 953–961. DOI: 10.1016/j.atmosenv.2003.11.001.

Widory D., Liu X.D., Dong S.P., 2010. Isotopes as tracers of sources of lead and strontium in aerosols (TSP & PM2.5) in Beijing. Atmos. Environ. 44, 3679-3687. DOI: 10.1016/j.atmosenv.2010.06.036.

World Health Organization (WHO), 2007. Population health and waste management: scientific data and policy options. Report of a WHO workshop, Rome, Italy. Copenhagen, Denmark: Regional Office for Europe.

Xu L.L., Chen X.Q., Chen J.S., Zhang F.W., He C., Zhao J.P., Yin L.Q., 2012. Seasonal variations and chemical compositions of PM2.5 aerosol in the urban area of Fuzhou, China. Atmos. Res. 104-105, 264-272. DOI: 10.1016/j.atmosres.2011.10.017.

Xu H.M., He K.L., Feng R., Shen Z.X., Cao J.J., Liu S.X., Ho K.F., Huang R.-J., Guinot B., Wang Q.Y., Zhou J.M., Shen M. X., Xiao S., Zhouf B.H., Sonke J.E., 2020. Metallic elements and Pb isotopes in PM2.5 in three Chinese typical megacities: spatial distribution and source apportionment. Environ. Sci.: Processes Impacts 22, 1718-1730. DOI: 10.1039/d0em00174k.

Yadav R., Sahu L.K., Jaaffrey S.N.A., Beig G., 2014. Distributions of ozone and related trace gases at an urban site in western India. J. Atmos. Chem. 71, 125–144. DOI: 10.1007/s10874-014-9286-9.

Zhang J., Peng J., Song C., Ma C., Men Z., Wu J., Wu L., Wang T., Zhang X., Tao S., Gao S., Hopke P.K., Mao H., 2020. Vehicular non-exhaust particulate emissions in Chinese megacities: Source profiles, real-world emission factors, and inventories. Environ. Pollut. 266, 115268 DOI: 10.1016/j.envpol.2020.115268.

Zhao Y., Yu R.L., Hu G.R., Lin X.H., Liu X.R., 2017. Chemical characteristics and Pb isotopic compositions of PM2.5 in Nanchang, China. Particuology 32, 95–102. DOI: 10.1016/j.partic.2016.07.009.

Zhao L., Hu G., Yan Y., Yu R., Cui J., Wang X., Yan Y., 2019. Source apportionment of heavy metals in urban road dust in a continental city of eastern China: Using Pb and Sr isotopes combined with multivariate statistical analysis. Atmos. Environ. 201, 201–211. DOI: 10.1016/j.atmosenv.2018.12.050.

Zhou J.B., Xing Z.Y., Deng J.J., Du K., 2016. Characterizing and sourcing ambient PM2.5 over key emission regions in China I: water-soluble ions and carbonaceous fractions. Atmos. Environ. 135, 20-30. DOI: 10.1016/j.atmosenv.2016.03.054.

Zhou J.M., Shen M.X., Xiao S., Zhou B.H., Sonke J.E., 2020. Metallic elements and Pb isotopes in $PM_{2.5}$ in three Chinese typical megacities: spatial distribution and source apportionment. Environ. Sci.-Proc. Imp. 22, 1718-1730. DOI: 10.1039/d0em00174k.

Zhu Y., Kashiwagi K., Sakaguchi M., Aoki M., Fujimori E., Haraguchi H., 2006. Lead isotopic compositions of atmospheric suspended particulate matter in Nagoya City as measured by HR-ICP-MS. J. Nucl. Sci. Technol. 43, 474-478. DOI: 10.3327/jnst.43.474.

SUPPLEMENTARY MATERIAL

Table 1S. Meteorological data, PM_{10} and $PM_{2.5}$ mass concentrations (µg/m^3), and NO and NO_2 atmospheric concentrations (µg/m^3) of the samples collected during start-up phase: a) from 09 May 2013 to 17 June 2013 and b) from 18 June 2013 to 16 July 2013.

a)	$PM_{2.5}$	PM_{10}	NO	NO_2	WS avg (m/s)	WS max (m/s)	h avg (m)	h max (m)	T avg (°C)
09/05	n.a.	21	129	603	1.03	2.15	688	1419	19.08
10/05	10	14	47	459	1.06	1.85	611	1305	16.31
11/05	8	9	110	327	0.82	1.54	625	1370	17.27
12/05	5	8	37	126	1.00	2.24	737	1465	17.79
13/05	8	13	268	782	0.86	1.76	647	1316	16.56
14/05	12	16	72	597	1.04	2.15	686	1380	16.17
15/05	7	11	39	501	1.66	2.60	642	1281	12.08
16/05	3	6	99	620	1.83	2.73	562	1186	11.41
25/05	5	5	46	336	1.34	2.47	567	1230	10.58
26/05	6	5	71	438	1.19	1.74	631	1262	14.24
27/05	9	11	99	509	1.16	2.54	607	1313	15.41
28/05	11	20	77	396	0.88	1.79	561	1246	14.28
29/05	5	6	88	498	1.28	1.94	685	1360	12.37
30/05	5	9	255	670	1.16	1.83	585	1279	14.32
31/05	6	6	235	598	1.28	1.86	602	1278	16.62
01/06	9	14	102	433	0.87	1.42	594	1269	19.34
02/06	7	49	58	422	0.88	1.43	726	1438	21.14
03/06	16	19	n.a.	849	0.79	1.50	670	1320	18.27
04/06	15	21	132	942	0.69	1.05	630	1236	19.17
05/06	18	26	102	923	0.64	1.44	601	1326	19.14
08/06	14	21	76	652	0.81	1.93	579	1297	20.22
09/06	8	13	42	303	1.16	2.50	607	1209	15.33
10/06	8	11	119	522	0.83	1.31	587	1220	17.59
11/06	9	15	181	909	0.67	1.21	678	1400	21.14
14/06	20	33	68	735	0.83	1.75	730	1380	23.73
15/06	21	32	51	548	1.02	2.05	739	1459	23.50
16/06	16	23	45	331	1.03	1.50	719	1417	24.38
17/06	19	31	107	729	0.67	1.14	615	1255	26.18

b)	$PM_{2.5}$	PM_{10}	NO	NO_2	WS avg (m/s)	WS max (m/s)	h avg (m)	h max (m)	T avg (°C)
18/06	22	36	74	677	0.68	1.07	618	1276	27.13
19/06	21	33	64	618	0.73	1.23	547	1210	26.1
20/06	17	27	131	784	0.92	1.77	559	1203	21.47
21/06	15	21	104	485	0.86	1.42	700	1386	21.40
22/06	12	18	65	411	1.07	1.58	732	1457	22.43
24/06	4	10	62	503	1.15	2.82	837	1562	21.45
25/06	5	8	152	1072	0.79	1.25	783	1567	20.58
26/06	6	12	138	838	0.87	1.57	786	1555	20.55
27/06	11	17	56	656	1.22	2.03	730	1462	17.44
28/06	11	15	68	530	0.88	1.47	678	1401	16.46
29/06	13	21	166	777	0.84	1.60	696	1433	18.22
30/06	11	18	n.a.	593	0.85	1.65	705	1452	21.61
02/07	12	23	101	476	0.76	1.66	790	1949	22.67
03/07	14	21	n.a.	595	0.88	1.71	708	1444	21.00
04/07	15	23	241	761	0.78	1.37	717	1422	23.40
05/07	16	26	117	914	0.62	1.21	757	1507	25.30
06/07	18	27	42	490	0.87	1.92	725	1492	25.36
07/07	15	21	11	326	1.08	1.63	658	1405	25.31
08/07	15	22	93	490	0.76	1.36	662	1376	24.65
09/07	11	16	117	542	0.81	1.27	592	1301	23.86
10/07	13	21	123	815	0.62	1.10	666	1383	24.39
11/07	14	23	56	553	0.74	1.79	711	1388	25.23
12/07	18	29	48	529	0.75	1.95	682	1326	23.71
13/07	21	31	n.a.	466	0.85	1.66	671	1293	24.22
14/07	16	19	32	316	0.70	1.23	639	1370	23.95
15/07	17	22	187	708	0.51	0.91	663	1428	25.24
16/07	20	27	43	470	0.94	1.69	649	1375	24.95

WS avg = average wind speed; WS max = maximum wind speed; WD = wind direction; h avg = average mixing height; h max = maximum mixing height; T avg = average temperature.

Table 2S. Experimental conditions, limits of detection (LOD) and sample blank concentrations of the analytes determined by ICP-AES.

Analyte	LOD (μg/L)	Sample Blank A (μg/L)	Sample Blank B (μg/L)
Al 396.153	8.1	45	46
Ca 317.933	40.8	100	90
Fe 238.204	39.8	< LOD	< LOD
K 769.896	5.2	30	20
Mg 285.213	8.6	32	31
Mn 257.610	0.22	2.1	1.0
K 769.896	5.2	30	20

A: Millipore© filters; B: Munktell filters

Table 3S. Experimental conditions, limits of detection (LOD) and sample blank concentrations of the analytes determined by SF-ICP-MS

Analyte	LOD (ng/L)	Sample Blank A (ng/L)	Sample Blank B (ng/L)
Ti47(LR)	754	3,860	1,030
V51(LR)	12	58	90
Cr53(LR)	48	834	760
Co59(MR)	7.0	8.7	< LOD
Ni60(MR)	41	240	350
Cu63(LR)	583	< LOD	< LOD
Zn66(MR)	1,450	3,860	3,220
As75(LR)	13	< LOD	< LOD
Sn118(LR)	3.0	< LOD	< LOD
Zr90(LR)	12	660	620
Mo96(MR)	21	390	340
Cd111(LR)	6.0	9.6	< LOD

Ba138(LR)	253	910	1,360
La139(MR)	5.7	62	60
Ce140(MR)	2.0	260	300
Tl203(MR)	14	< LOD	< LOD
Pb208(LR)	13	68	53

LR = Low Resolution; MR = Medium Resolution; A: Millipore© filters; B: Munktell filters

Table 4S. Limits of detection (LOD) and sample blank concentrations of water-soluble ions determined by IC.

Analyte	**LOD (μg/L)**	**Sample Blank A (μg/L)**	**Sample Blank B (μg/L)**
Cl^-	50	< LOD	< LOD
NO_3^-	500	< LOD	< LOD
SO_4^{2-}	800	< LOD	< LOD
Na^+	250	< LOD	< LOD
K^+	200	< LOD	< LOD
Mg^{2+}	150	< LOD	< LOD
Ca^{2+}	900	< LOD	< LOD
NH_4^+	100	< LOD	< LOD

A: Millipore© filters; B: Munktell filters

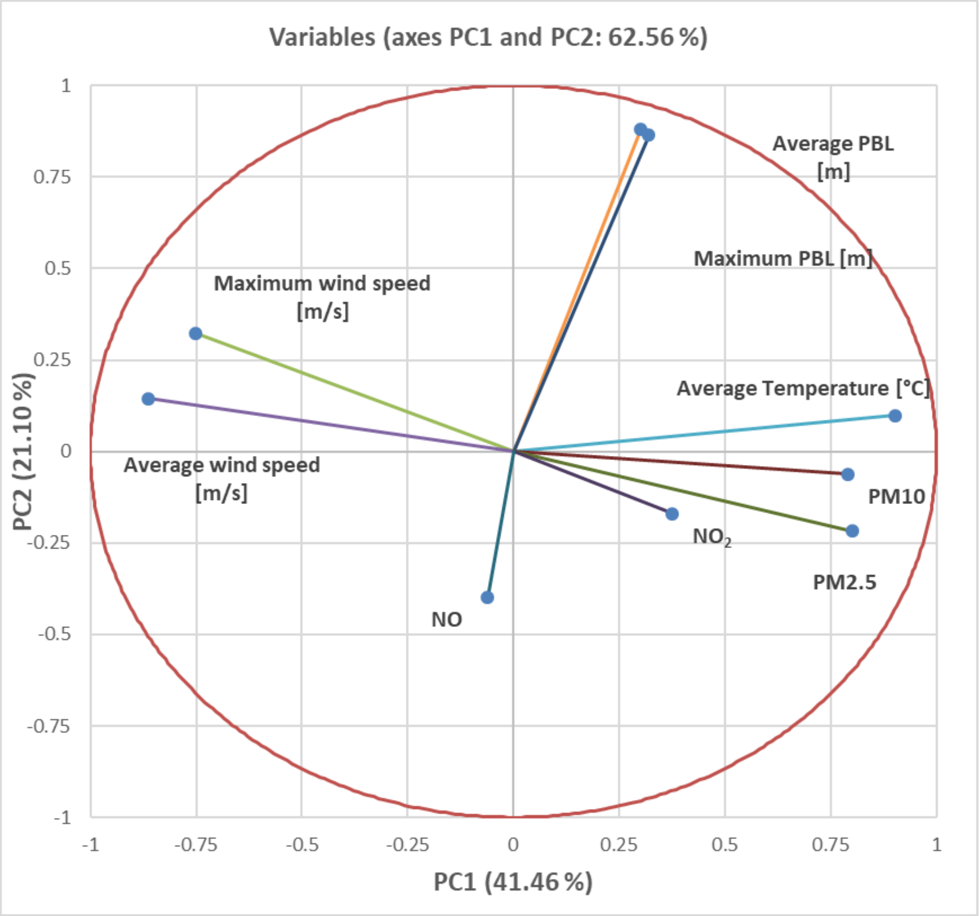

Figure 1S. Loadings from PCA (Principal Components Analysis).

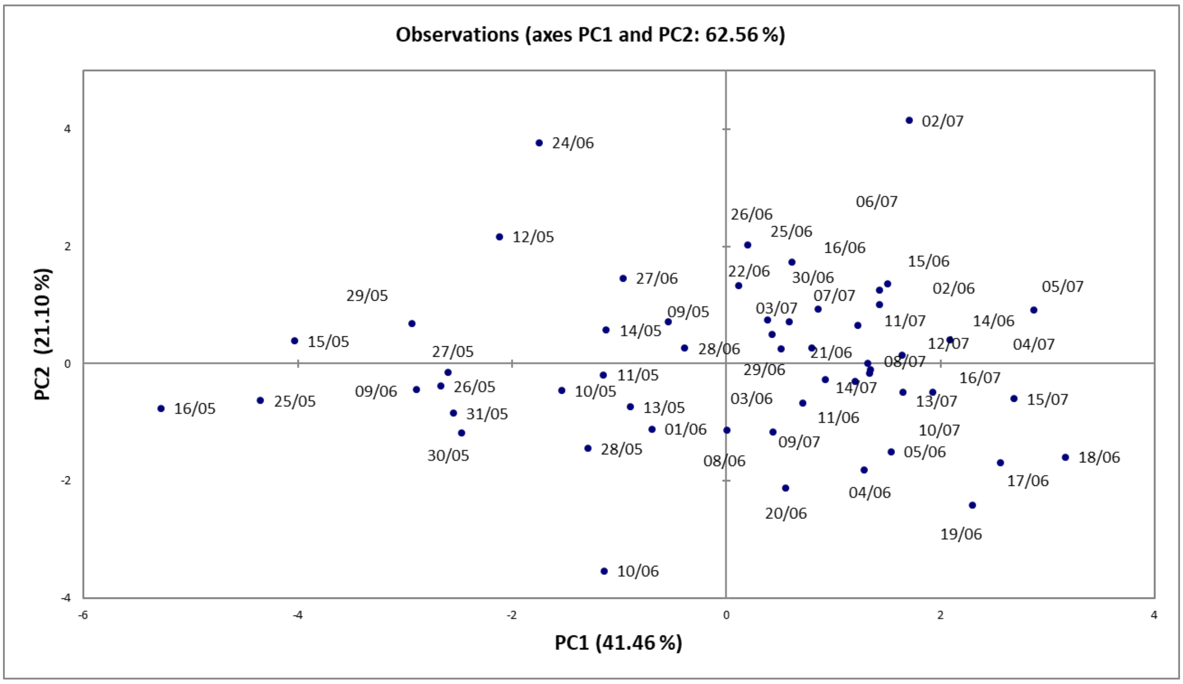

Figure 2S. Scores from PCA (Principal Components Analysis).

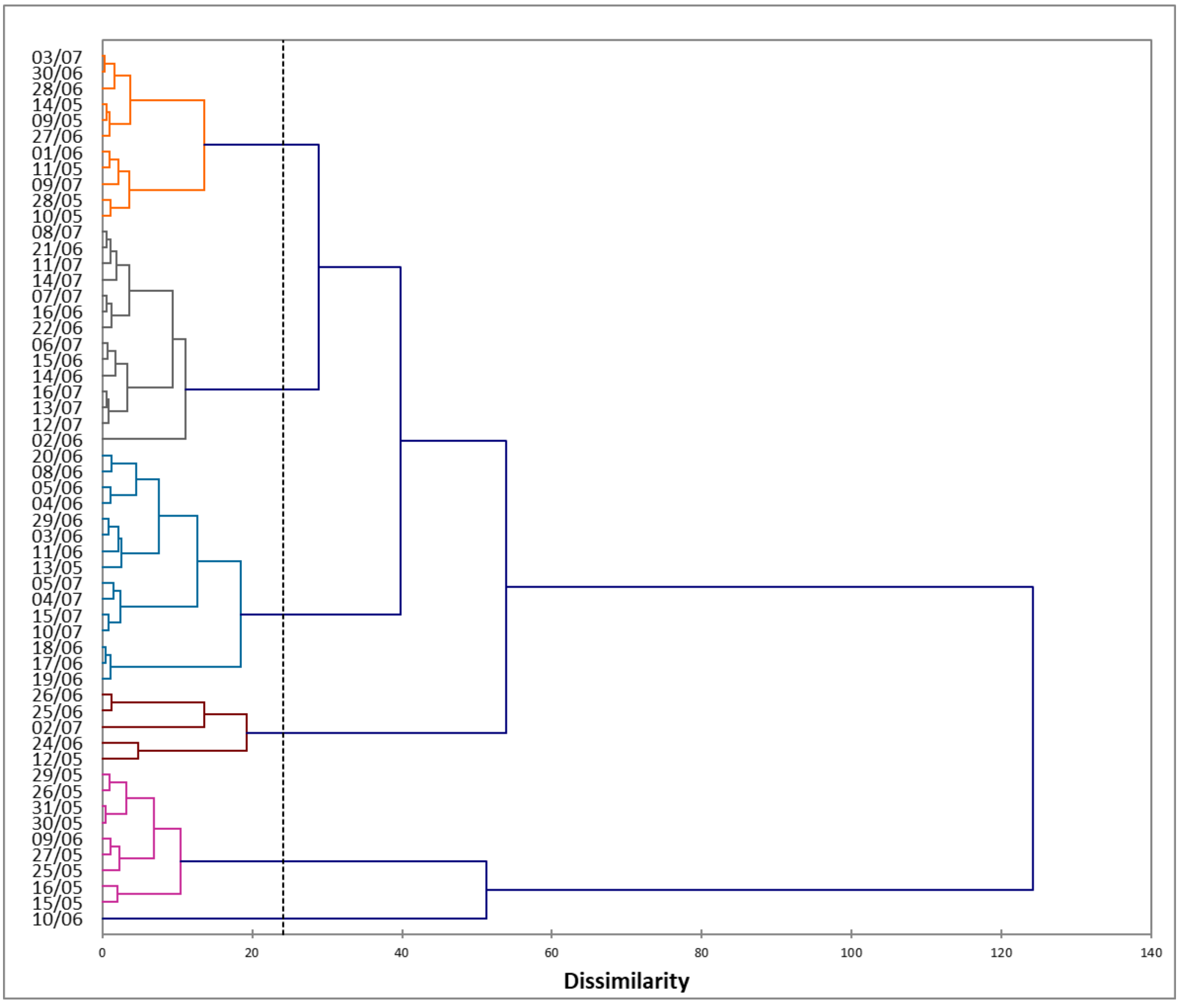

Figure 3S. Dendrogram of the samples from HCA (Hierarchical Cluster Analysis).

Table 5S. Water-soluble ionic components and major element concentrations in PM_{10} samples. All the results are expressed in ng/m^3, except NH_4^+, NO_3^- and SO_4^{2-} which are expressed in $\mu g/m^3$.

	Al	**Ca**	**Ca^{2+}**	**Cl^-**	**Fe**	**K**	**K^+**	**Mg**	**Mg^{2+}**	**Na**	**Na^+**	**NH_4^+**	**NO_3^-**	**SO_4^{2-}**
25 May	108 ± 1	178 ± 7	191 ± 8	< 19	200 ± 3	36 ± 2	40 ± 2	88 ± 2	12.7 ± 0.4	< SB	31 ± 1	0.26 ± 0.01	5.1 ± 0.2	0.64 ± 0.02
26 May	127 ± 4	147 ± 5	103 ± 3	< 19	233 ± 1	76.5 ± 0.2	84 ± 3	85.8 ± 0.2	10.6 ± 0.5	15 ± 5	29 ± 1	0.17 ± 0.01	4.9 ± 0.2	0.253 ±0.007
27 May	230 ± 30	350 ± 40	280 ± 10	320 ± 10	340 ± 30	140 ± 20	100 ± 4	260 ± 30	116 ± 4	840 ± 30	950 ± 40	0.39 ± 0.01	19.6 ± 0.9	2.1 ± 0.1
28 May	217 ± 4	340 ± 20	330 ± 20	42 ± 1	332 ± 5	117 ± 3	105 ± 4	230 ± 4	86 ± 4	520 ± 20	680 ± 20	0.78 ± 0.02	27 ± 1	2.13 ± 0.08
29 May	101 ± 3	175 ± 2	156 ± 6	< 19	235 ± 8	46 ± 5	63 ± 2	81 ± 4	12.7 ± 0.5	27 ± 1	50 ± 2	0.180 ± 0.007	7.2 ± 0.3	0.32 ± 0.01
30 May	85 ± 3	137 ± 1	107 ± 5	21.0 ± 0.8	299 ± 8	54 ± 1	71 ± 2	72 ± 5	10.5 ± 0.4	< SB	29 ± 1	0.127 ± 0.007	4.8 ± 0.2	0.34 ± 0.01
31 May	210 ± 10	311 ± 6	250 ± 10	42 ± 2	375 ± 1	103 ± 5	75 ± 2	170 ± 3	36 ± 1	106 ± 1	136 ± 5	0.163 ± 0.008	6.5 ± 0.3	0.54 ± 0.02
14 June	690 ± 10	680 ± 5	770 ± 30	20.9 ± 0.8	800 ± 10	320 ± 10	131 ± 4	423 ± 2	67 ± 2	136 ± 1	123 ± 5	1.29 ± 0.06	34 ± 1	1.80 ± 0.06
15 June	401 ± 2	470 ± 10	540 ± 20	20.9 ± 0.7	540 ± 10	210 ± 5	102 ± 3	251 ± 2	61 ± 2	133 ± 2	154 ± 6	2.01 ± 0.09	55 ± 2	1.82 ± 0.06
16 June	195 ± 1	243 ± 20	290 ± 10	20.9 ± 0.6	294 ± 4	133 ± 1	97 ± 4	125 ± 1	35 ± 1	80 ± 2	108 ± 5	1.78 ± 0.08	54 ± 2	0.67 ± 0.03
17 June	520 ± 20	610 ± 10	700 ± 30	< 19	660 ± 20	258 ± 1	110 ± 5	353 ± 9	65 ± 2	146 ± 1	141 ± 6	1.75 ± 0.09	52 ± 2	1.15 ± 0.06
18 June	680 ± 20	780 ± 30	740 ± 30	20.9 ± 0.8	870 ± 20	310 ± 10	138 ± 5	454 ± 3	65 ± 3	168 ± 7	132 ± 6	1.76 ± 0.05	51 ± 2	1.56 ± 0.06
19 June	610 ± 60	818 ± 9	850 ± 20	20.9 ± 0.9	780 ± 20	310 ± 30	165 ± 6	370 ± 10	63 ± 2	157 ± 7	100 ± 4	1.53 ± 0.07	46 ± 2	1.37 ± 0.05
20 June	234 ± 6	420 ± 20	490 ± 20	21.1 ± 0.8	469 ± 1	214 ± 1	198 ± 5	167 ± 9	42 ± 1	138 ± 1	116 ± 4	1.46 ± 0.06	41 ± 1	2.11 ± 0.08
02 July	430 ± 20	478 ± 9	550 ± 20	< 19	490 ± 9	218 ± 9	90 ± 4	269 ± 6	42 ± 1	100 ± 4	69 ± 2	0.83 ± 0.02	23 ± 1	0.93 ± 0.04
05 July	570 ± 30	550 ± 20	660 ± 20	< 19	750 ± 20	292 ± 9	126 ± 6	360 ± 10	54 ± 2	122 ± 2	75 ± 3	0.87 ± 0.05	24 ± 1	1.29 ± 0.05
06 July	408 ± 6	490 ± 6	570 ± 20	< 19	530 ± 10	212 ± 3	80 ± 4	276 ± 5	52 ± 2	109 ± 2	67 ± 2	1.32 ± 0.06	36 ± 1	1.16 ± 0.05
07 July	290 ± 10	324 ± 2	310 ± 10	< 19	350 ± 10	161 ± 5	80 ± 3	170 ± 10	27 ± 1	95 ± 6	52 ± 3	1.22 ± 0.05	34 ± 1	0.78 ± 0.03
10 July	235 ± 1	302 ± 1	380 ± 10	< 19	428 ± 1	146 ± 1	100 ± 5	157 ± 2	44 ± 1	30 ± 2	35 ± 2	0.77 ± 0.04	22 ± 1	0.74 ± 0.04
11 July	310 ± 20	280 ± 10	330 ± 20	< 19	390 ± 20	168 ± 10	77 ± 4	180 ± 10	35 ± 1	45 ± 2	31 ± 1	0.88 ± 0.03	28 ± 1	0.84 ± 0.03
14 July	143 ± 4	139 ± 1	175 ± 8	21.0 ± 0.8	199 ± 3	140 ± 10	109 ± 4	74 ± 1	21 ± 1	59 ± 1	59 ± 2	1.13 ± 0.04	27 ± 1	0.43 ± 0.02
15 July	223 ± 4	270 ± 10	316 ± 9	21 ± 1	381 ± 4	160 ± 1	117 ± 4	153 ± 2	36 ± 2	53 ± 5	50 ± 2	0.91 ± 0.03	24 ± 1	0.49 ± 0.03

SB: Sample Blank

Table 6S. Minor and trace element (Ba, Cr, Cu, Mn, Ni, Pb, Sn, Ti, V and Zn) concentrations in PM$_{10}$ samples. All the results are expressed in ng/m^3.

	Ba	**Cr**	**Cu**	**Mn**	**Ni**	**Pb**	**Sn**	**Ti**	**V**	**Zn**
25 May	4.36 ± 0.07	< SB	7.5 ± 0.1	5.304 ± 0.007	0.95 ± 0.08	0.76 ± 0.01	2.3 ± 0.2	4.16 ± 0.08	0.27 ± 0.01	8.6 ± 0.3
26 May	4.8 ± 0.1	< SB	10.7 ± 0.5	5.384 ± 0.007	0.87 ± 0.07	0.88 ± 0.03	3 ± 1	3.33 ± 0.09	0.27 ± 0.01	8.6 ± 0.1
27 May	6.1 ± 0.7	0.59 ± 0.09	11.7 ± 0.4	6.3 ± 0.2	2.0 ± 0.4	1.7 ± 0.2	2.9 ± 0.2	7 ± 1	1.7 ± 0.1	14 ± 1
28 May	6.0 ± 0.2	1.23 ± 0.09	9.7 ± 0.9	6.63 ± 0.09	2.62 ± 0.02	2.27 ± 0.06	3.7 ± 0.3	6.7 ± 0.3	2.27 ± 0.03	13 ± 1
29 May	5.6 ± 0.8	0.042 ± 0.002	9.42 ± 0.09	5.63 ± 0.04	1.22 ± 0.02	0.79 ± 0.08	1.5 ± 0.1	4.4 ± 0.7	0.54 ± 0.03	17.0 ± 0.8
30 May	7 ± 1	0.199 ± 0.005	7.3 ± 0.3	5.9 ± 0.3	1.20 ± 0.04	0.54 ± 0.03	2.7 ± 0.3	4.0 ± 0.2	0.23 ± 0.01	22.8 ± 0.3
31 May	8.2 ± 0.3	1.26 ± 0.05	9.4 ± 0.3	8.95 ± 0.04	2.04 ± 0.03	1.22 ± 0.01	3.7 ± 0.1	7.2 ± 0.5	0.66 ± 0.03	18.1 ± 0.3
14 June	14.9 ± 0.1	6.9 ± 0.8	23.0 ± 0.2	30 ± 1	4.9 ± 0.5	7.35 ± 0.07	6.32 ± 0.09	22 ± 1	2.27 ± 0.04	33.7 ± 0.8
15 June	10.4 ± 0.3	1.93 ± 0.02	17.3 ± 0.4	34 ± 2	3.66 ± 0.06	6.1 ± 0.2	6.5 ± 0.3	12.6 ± 0.5	3.8 ± 0.1	23 ± 2
16 June	5.6 ± 0.3	0.089 ± 0.005	10.9 ± 0.2	9.03 ± 0.08	2.85 ± 0.06	2.73 ± 0.08	4.1 ± 0.4	5.4 ± 0.2	4.39 ± 0.05	9.0 ± 0.2
17 June	11.4 ± 0.3	3.25 ± 0.07	19.2 ± 0.3	21.67 ± 0.03	4.4 ± 0.1	4.75 ± 0.05	5.46 ± 0.08	13.0 ± 0.4	3.90 ± 0.07	22.4 ± 0.5
18 June	46.6 ± 0.6	6.0 ± 0.2	21.0 ± 0.7	22.6 ± 0.4	4.8 ± 0.1	4.6 ± 0.1	5.9 ± 0.4	20.6 ± 0.9	3.2 ± 0.1	25.6 ± 0.9
19 June	59 ± 3	5.5 ± 0.7	19.58 ± 0.02	20.9 ± 0.6	3.9 ± 0.2	5.0 ± 0.2	5.0 ± 0.3	20 ± 3	2.5 ± 0.1	49 ± 2
20 June	63 ± 5	3.1 ± 0.1	18.9 ±0.4	33 ± 7	2.54 ± 0.03	3.2 ± 0.1	4.5 ± 0.2	7.70 ± 0.07	1.94 ± 0.04	43 ± 2
02 July	43.5 ± 0.8	3.6 ± 0.5	14.0 ± 0.5	13.93 ± 0.01	2.9 ± 0.1	3.76 ± 0.06	3.6 ± 0.3	12.9 ± 0.8	1.5 ± 0.1	40 ± 10
05 July	43 ± 1	4.5 ± 0.2	22.1 ± 0.5	21.2 ± 0.7	3.80 ± 0.09	4.4 ± 0.1	5.4 ± 0.2	16 ± 1	1.67 ± 0.08	28.1 ± 0.4
06 July	43 ± 1	3.4 ± 0.1	15 ± 1	20.9 ± 0.1	2.77 ± 0.09	3.5 ± 0.8	4.3 ± 0.6	17 ± 3	1.31 ± 0.07	37 ± 2
07 July	52.0 ± 0.3	1.92 ± 0.07	11 ± 1	19 ± 2	1.8 ± 0.2	3.50 ± 0.03	3.36 ± 0.03	9.6 ± 0.6	0.87 ± 0.01	36.2 ± 0.1
10 July	< SB	4.1 ± 0.1	14.67 ± 0.08	9.9 ± 0.2	2.2 ± 0.2	2.57 ± 0.02	4.10 ± 0.05	8.1 ± 0.2	0.66 ± 0.02	10.8 ± 0.1
11 July	< SB	4.7 ± 0.5	13.1 ± 0.2	11.6 ± 0.6	2.1 ± 0.3	3.0 ± 0.2	3.61 ± 0.08	10 ± 1	0.81 ± 0.05	13.9 ± 0.4
14 July	11.6 ± 0.1	1.48 ± 0.02	8.8 ± 0.2	8.1 ± 0.5	1.47 ± 0.01	2.26 ± 0.02	2.48 ± 0.03	5.5 ± 0.4	1.45 ± 0.01	13.6 ± 0.4
15 July	16.5 ± 0.4	2.54 ± 0.02	15.1 ± 0.8	9.20 ± 0.02	1.9 ± 0.1	2.37 ± 0.05	4.73 ± 0.07	6.8 ± 0.2	1.10 ± 0.01	18.6 ± 0.1

SB: Sample Blank

Table 7S. Trace element (As, Cd, Ce, Co, La, Mo, Tl and Zr) concentrations in PM$_{10}$ samples. All the results are expressed in pg/m^3.

	As	**Cd**	**Ce**	**Co**	**La**	**Mo**	**Tl**	**Zr**
25 May	540 ± 10	34 ± 1	113 ± 8	36 ± 2	87 ± 2	178 ± 7	2.2 ± 0.2	334 ± 17
26 May	600 ± 40	30 ± 4	130 ± 9	25.3 ± 0.7	80 ± 3	217 ± 1	4.0 ± 0.6	340 ± 7
27 May	630 ± 30	35 ± 3	210 ± 20	141 ± 4	140 ± 10	290 ± 20	7.4 ± 0.7	420 ± 50
28 May	625 ± 7	58 ± 1	270 ± 10	168 ± 4	170 ± 10	380 ± 5	7.43 ± 0.03	318 ± 2
29 May	560 ± 20	34 ± 2	92 ± 3	47 ± 2	63.9 ± 0.5	256 ± 5	2.0 ± 0.2	280 ± 10
30 May	593 ± 6	23.6 ± 0.7	80 ± 5	48 ± 6	55 ± 4	450 ± 10	1.78 ± 0.08	510 ± 20
31 May	700 ± 30	129 ± 2	220 ± 10	74 ± 2	124 ± 5	458 ± 3	4.6 ± 0.2	650 ± 30
14 June	1300 ± 100	99 ± 2	770 ± 40	189 ± 8	590 ± 20	1040 ± 10	17.4 ± 0.4	1070 ± 50
15 June	1020 ± 40	90 ± 3	460 ± 10	99 ± 1	388 ± 9	710 ± 20	17.1 ± 0.6	700 ± 10
16 June	780 ± 20	49 ± 2	194 ± 9	50.2 ± 0.2	187 ± 1	485 ± 7	12.0 ± 0.5	380 ± 10
17 June	890 ± 10	69 ± 2	530 ± 20	1060 ± 20	382 ± 9	753 ± 7	16.9 ± 0.2	860 ± 10
18 June	590 ± 10	114 ± 3	618 ± 20	222 ± 3	412 ± 3	930 ± 30	16.3 ± 0.8	1020 ± 40
19 June	569 ± 1	88 ± 3	530 ± 20	210 ± 20	370 ± 10	960 ± 40	24.1 ± 0.9	1000 ± 100
20 June	413 ± 8	82 ± 2	111 ± 1	112 ± 1	119 ± 1	840 ± 20	26.0 ± 0.8	860 ± 10
02 July	345 ± 9	63 ± 3	352 ± 6	130 ± 3	258 ± 3	529 ± 4	10.3 ± 0.3	520 ± 20
05 July	444 ± 6	73 ± 4	450 ± 20	164 ± 5	400 ± 10	910 ± 30	11.7 ± 0.4	820 ± 80
06 July	560 ± 20	91 ± 5	250 ± 10	104 ± 2	320 ± 10	770 ± 50	14.6 ± 0.8	460 ± 40
07 July	490 ± 10	90 ± 2	109 ± 5	63 ± 5	186 ± 3	503 ± 7	15.3 ± 0.3	390 ± 10
10 July	383 ± 4	68 ± 2	85.6 ± 0.2	74 ± 3	85 ± 2	850 ± 20	12.3 ± 0.2	640 ± 10
11 July	390 ± 20	74 ± 4	130 ± 10	97 ± 7	150 ± 10	740 ± 40	14.5 ± 0.9	450 ± 40
14 July	280 ± 4	68 ± 3	< SB	38.6 ± 0.7	165 ± 3	420 ± 6	11.8 ± 0.3	260 ± 4
15 July	353 ± 7	79 ± 3	83 ± 1	95 ± 4	148 ± 4	680 ± 10	10.5 ± 0.2	530 ± 3

SB: Sample Blank

Table 8S: Lead isotope ratios (namely $^{204}Pb/^{206}Pb$, $^{206}Pb/^{207}Pb$ and $^{208}Pb/^{206}Pb$ ratios) for PM_{10} samples collected during start-up phase of the incinerator.

	^{204}**Pb/**^{206}**Pb**	^{206}**Pb/**^{207}**Pb**	^{208}**Pb/**^{206}**Pb**
	Mean ± SD	**Mean ± SD**	**Mean ± SD**
25 May	0.0541 ± 0.0005	1.1532 ± 0.0003	2.1228 ± 0.0006
26 May	0.0538 ± 0.0004	1.1601 ± 0.0002	2.1186 ± 0.0004
27 May	0.0526 ± 0.0004	1.1488 ± 0.0002	1.8633 ± 0.0009
28 May	0.0516 ± 0.0006	1.1597 ± 0.0009	1.8453 ± 0.0012
29 May	0.0536 ± 0.0004	1.1685 ± 0.0005	2.0825 ± 0.0012
30 May	0.0532 ± 0.0001	1.1626 ± 0.0006	2.0922 ± 0.0001
31 May	0.0531 ± 0.0001	1.1635 ± 0.0006	2.1180 ± 0.0005
14 June	0.0565 ± 0.0002	1.1643 ± 0.0009	2.0561 ± 0.0018
15 June	0.0551 ± 0.0006	1.1642 ± 0.0003	2.0176 ± 0.0003
16 June	0.0519 ± 0.0003	1.1677 ± 0.0005	1.9363 ± 0.0001
17 June	0.0543 ± 0.0006	1.1308 ± 0.0002	2.0266 ± 0.0008
18 June	0.0557 ± 0.0002	1.1370 ± 0.0009	2.0212 ± 0.0014
19 June	0.0566 ± 0.0002	1.1686 ± 0.0001	2.0159 ± 0.0025
20 June	0.0514 ± 0.0006	1.1721 ± 0.0003	1.8929 ± 0.0041
02 July	0.0522 ± 0.0004	1.1363 ± 0.0009	1.9752 ± 0.0007
05 July	0.0535 ± 0.0003	1.1344 ± 0.0011	2.0354 ± 0.0015
06 July	0.0530 ± 0.0008	1.1448 ± 0.0012	1.9576 ± 0.0043
07 July	0.0501 ± 0.0004	1.2073 ± 0.0005	1.8884 ± 0.0015
10 July	0.0512 ± 0.0003	1.1883 ± 0.0007	1.9085 ± 0.0002
11 July	0.0504 ± 0.0004	1.1933 ± 0.0008	1.8789 ± 0.0039
14 July	0.0505 ± 0.0003	1.1962 ± 0.0005	1.9126 ± 0.0014
15 July	0.0504 ± 0.0001	1.2118 ± 0.0009	1.8836 ± 0.0006